JPEDAV (2004) 25:329-345
DOI: 10.1361/15477030420106
1547-7037/$19.00 ©ASM International

Critical Thermodynamic Evaluation and Optimization of the $MgO-Al_2O_3$, $CaO-MgO-Al_2O_3$, and $MgO-Al_2O_3-SiO_2$ Systems

In-Ho Jung, Sergei A. Decterov, and Arthur D. Pelton

(Submitted November 13, 2003; in revised form May 25, 2004)

A complete literature review, critical evaluation, and thermodynamic modeling of the phase diagrams and thermodynamic properties of all oxide phases in the $MgO-Al_2O_3$, $CaO-MgO-Al_2O_3$, and $MgO-Al_2O_3-SiO_2$ systems at 1 bar total pressure are presented. Optimized model equations for the thermodynamic properties of all phases are obtained that reproduce all available thermodynamic and phase equilibrium data within experimental error limits from 25 °C to above the liquidus temperatures at all compositions. The database of the model parameters can be used along with software for Gibbs energy minimization to calculate all thermodynamic properties and any type of phase diagram section. The modified quasichemical model was used for the liquid slag phase and sublattice models, based upon the compound energy formalism, were used for the spinel, pyroxene, and monoxide solid solutions. The use of physically reasonable models means that the models can be used to predict thermodynamic properties and phase equilibria in composition and temperature regions where data are not available.

1. Introduction

The $MgO-Al_2O_3$, $CaO-MgO-Al_2O_3$, and $MgO-Al_2O_3-SiO_2$ systems are fundamental to the understanding of metallurgical slags, refractories, ceramic materials, and geological phenomena. Eriksson et al.[1] reported a thermodynamic evaluation/optimization of the $MgO-Al_2O_3$ system using a simplified model for the spinel solution. Hallstedt[2] described the spinel solution using a three-sublattice (three cation sublattices plus the oxygen sublattice) Compound Energy Formalism in his optimization of the $MgO-Al_2O_3$ system. He modeled the liquid slag using a two-sublattice ionic model. Hallstedt also reported an optimization of the ternary $CaO-MgO-Al_2O_3$ system.[3]

Recently, a new formulation of the spinel model[4] was developed. Furthermore, many new structural and thermodynamic data for the spinel phase have been reported, and two new ternary phases in the $CaO-MgO-Al_2O_3$ system have been reported. A new and more accurate thermodynamic optimization/evaluation of the $MgO-Al_2O_3$ and $CaO-MgO-Al_2O_3$ systems, using the most recent models and data, is warranted. A thermodynamic evaluation/optimization of the $MgO-Al_2O_3-SiO_2$ system has not previously been reported.

The main goal of the current study is to perform a complete review, critical assessment, and optimization of thermodynamic properties at 1 bar total pressure of oxide phases in the $MgO-Al_2O_3$, $CaO-MgO-Al_2O_3$, and $MgO-Al_2O_3-SiO_2$ systems. In the thermodynamic "optimization" of a chemical system, all available thermodynamic and phase equilibrium data are evaluated simultaneously to obtain one set of model equations for the Gibbs energies of all phases as functions of temperature and composition. From these equations, all of the thermodynamic properties and the phase diagrams can be back-calculated. In this way, all the data are rendered self-consistent and consistent with thermodynamic principles. Thermodynamic property data, such as activity data, can aid in the evaluation of the phase diagram, and phase diagram measurements can be used to deduce thermodynamic properties. Discrepancies in the available data can often be resolved, and interpolations and extrapolations can be made in a thermodynamically correct manner.

The thermodynamic evaluation/optimization of the $MgO-Al_2O_3$, $CaO-MgO-Al_2O_3$, and $MgO-Al_2O_3-SiO_2$ systems reported in the current study is part of a wider research program aimed at complete characterization of phase equilibria and thermodynamic properties of the entire six-component system $CaO-MgO-Al_2O_3-FeO-Fe_2O_3-SiO_2$, which has numerous applications in the ceramic, cement, and glass industries, metallurgy, geochemistry, etc. The present optimization covers the range of temperatures from 25 °C to above the liquidus.

2. Phases and Thermodynamic Models

The following solution phases are found in the $CaO-MgO-Al_2O_3$ and $MgO-Al_2O_3-SiO_2$ systems:

Slag (molten oxide phase) $CaO-MgO-SiO_2-AlO_{1.5}$

Spinel $(Mg^{2+},Al^{3+})^{T}[Mg^{2+},Al^{3+},Va]_2^{O}O_4$

Pyroxene $(Mg)^{M2}(Mg^{2+},Al^{3+})^{M1}(Al^{3+},Si^{4+})^{B}(Si)^{A}O_6$

Monoxide $MgO-CaO-AlO_{1.5}$

In-Ho Jung, Sergei A. Decterov, and **Arthur D. Pelton,** Centre de Recherche en Calcul Thermochimique (CRCT) École Polytechnique de Montréal P.O. Box 6079, Station "Downtown" Montréal, PQ, Canada, H3C 3A7. Contact e-mail: arthur.pelton@polymtl.ca.

Cations shown within a set of brackets for spinel and pyroxene occupy the same sublattice.

2.1 Slag (Molten Oxide)

The modified quasichemical model,[5-8] which takes into account short-range-ordering of second-nearest-neighbor cations in the ionic melt, is used for modeling the slag. The subsystems CaO-MgO,[9] CaO-Al_2O_3,[10] MgO-SiO_2,[11] and Al_2O_3-SiO_2[10] have already been critically evaluated and optimized, and the optimized model parameters are used as the basis of the current study. All second-nearest-neighbor "coordination numbers" used in the model are the same as in the previous studies.[9-11] Additional binary and ternary model parameters for the MgO-Al_2O_3 and MgO-Al_2O_3-SiO_2 ternary slag solutions were optimized in the current study. These are listed in Table 1. The properties of the CaO-MgO-Al_2O_3 ternary solution were calculated from the binary parameters using an asymmetric "Toop-like" approximation[12] with $AlO_{1.5}$ as the "asymmetric" component, and the properties of the MgO-Al_2O_3-SiO_2 ternary solution were also calculated from the binary and ternary parameters using an asymmetric Toop-like approximation[12] with SiO_2 as the asymmetric component.

2.2 Compound Energy Formalism (CEF)

The spinel and pyroxene solution models were developed within the framework of the two-sublattice compound energy formalism (CEF).[13] (Although there are more than two sublattices, substitution occurs on only two cationic sublattices in each case.) The Gibbs energy expression in the CEF per formula unit is

$$G = \sum_i \sum_j Y_i' Y_j'' G_{ij} - TS_C + G^E \qquad \text{(Eq 1)}$$

where Y_i' and Y_j'' represent the site fractions of constituents i and j on the first and second sublattices, G_{ij} is the Gibbs energy of an end-member ij of the solution in which the first sublattice is occupied only by cation i and the second sublattice is occupied only by cation j, G^E is the excess Gibbs energy and S_C is the configurational entropy assuming random mixing on each sublattice:

$$S_C = -R\left(n_1 \sum_i Y_i' \ln Y_i' + n_2 \sum_j Y_j'' \ln Y_j'' \right) \qquad \text{(Eq 2)}$$

where n_1 and n_2 are the numbers of sites on the first and second sublattices per formula unit of a solution. G^E is expanded as

$$G^E = \sum_i \sum_j \sum_k Y_i' Y_j' Y_k'' L_{ij:k} + \sum_i \sum_j \sum_k Y_k' Y_i'' Y_j'' L_{k:ij} \qquad \text{(Eq 3)}$$

where the parameters $L_{ij:k}$ are related to interactions between cations i and j on the first sublattice when the second sublattice is occupied only by k cations, and the parameters $L_{k:ij}$ are related to interactions between i and j cations on the second sublattice when the first sublattice is occupied only by k cations.

2.2.1 Spinel Solution. The spinel solution is modeled as $(Mg^{2+},Al^{3+})^T[Mg^{2+},Al^{3+},Va]_2^O O_4$ with $n_1 = 1$ and $n_2 = 2$ sites on the tetrahedral and octahedral sublattices, respectively. Nonstoichiometry can occur through the introduction of vacancies, Va, on octahedral sites.

G^E was set to zero in the current study, so that the six end-member Gibbs energies G_{ij} are used to describe the system. Certain linear combinations of these end-member Gibbs energies, which have physical significance, are used as the optimized parameters as discussed in Ref 4. The optimized parameters are listed in Table 1. Details of the optimization are given in the following sections.

The parameter G_{MA} is equal to $G^o(MgAl_2O_4)$ the Gibbs energy of normal $MgAl_2O_4$ spinel. (The notations M, A, and V denote Mg^{2+}, Al^{3+}, and vacancy) The parameters I_{MA}, $\Delta_{MA:MA}$, and $\Delta_{MA:MV}$ are the Gibbs energy changes of the spinel inversion reaction and of reciprocal site exchange reactions, respectively.

The spinel solid solution can be considered as a solution of $MgAl_2O_4$ and γ-Al_2O_3: $(Al^{3+})(Al_{5/6}^{3+}Va_{1/6})_2O_4$. Assuming a random mixture of Al^{3+} and vacancies on the octahedral sites, the Gibbs energy of γ-Al_2O_3 is given by:

$$8G^\circ(\gamma\text{-}Al_2O_3) = G_{AV} + 5G_{AA} + 2RT(5 \ln 5 + 6 \ln 6) \qquad \text{(Eq 4)}$$

The Gibbs energy of γ-Al_2O_3 was optimized as equal to $G^o(\alpha\text{-}Al_2O_3)$ plus an increment as shown in Table 1.

Following O'Neill and Navrotsky[14] the parameter $\Delta_{MA:MA}$ was set to 40 kJ/mol. Since the current study is part of a larger study[15] of the entire Fe-Mg-Al-Cr-Co-Ni-Zn-O system, model parameters must be consistent with those obtained in optimization of other subsystems. The parameter G_{AA} was already optimized in evaluating the Fe-Al-O spinel solution. Similarly, $G^o(\gamma\text{-}Al_2O_3)$ must be optimized to simultaneously reproduce the solubilities of Al_2O_3 in all spinel solutions.

2.2.2 Pyroxene Solutions. In the absence of Ca, there are three polymorphs of pyroxene: ortho-pyroxene (*Pbca*, orthorhombic), proto-pyroxene (*Pbcn*, orthorhombic), and low clino-pyroxene (*P21/c*, monoclinic). All three are considered in the current study. Pyroxenes have two distinct octahedral sublattices (M1 and M2) and two distinct tetrahedral sublattices (A and B). Because the amount of Al on A sites is small,[16] the following simplified[17] pyroxene structure is used in the present model:

$$(Mg)^{M2}\,(Mg^{2+}, Al^{3+})^{M1}\,(Al^{3+}, Si^{4+})^{B}\,(Si)^{A}\,O_6 \qquad \text{(Eq 5)}$$

That is, mixing occurs only on the M1 and B sites, and so there are four end-member G_{ij} parameters in the model for each of the three polymorphs: G_{MA}, G_{MS}, G_{AA}, and G_{AS}

Table 1 Optimized Model Parameters of the CaO-MgO-Al_2O_3 and MgO-Al_2O_3-SiO_2 Systems (J/mol)

	$H^0_{298.15}$, J/mol	$S^0_{298.15}$ and C_P, J/mol · K
Ternary Compounds		
$Ca_3MgAl_4O_{10}$	–5 971 170.0	$S^0_{298.15} = 3\,S^0_{298.15}$ (CaO) + $S^0_{298.15}$ (MgO) + 2 $S^0_{298.15}$ (Al_2O_3) $C_P = 3C_P$(CaO) + C_P(MgO) + 2 C_P(Al_2O_3)
$CaMg_2Al_{16}O_{27}$	–15 438 690.0	$S^0_{298.15} = S^0_{298.15}$ (CaO) + 2 $S^0_{298.15}$ (MgO) + 8 $S^0_{298.15}$ (Al_2O_3) $C_P = C_P$(CaO) + 2 C_P(MgO) + 8 C_P(Al_2O_3)
$Ca_2Mg_2Al_{28}O_{46}$	–26 217 079.9	$S^0_{298.15} = 2\,S^0_{298.15}$ (CaO) + 2 $S^0_{298.15}$ (MgO) + 14 $S^0_{298.15}$ (Al_2O_3) $C_P = 2\,C_P$(CaO) + 2 C_P(MgO) + 14 C_P(Al_2O_3)
$Mg_2Al_4Si_5O_{18}$	–9 167 727.0	[97] $S^0_{298.15} = 417.9700$ [97] $C_P = 954.39 - 370\,210\,000T^{-3} - 2\,317\,300T^{-2} - 7962.3T^{-0.5}$
$Mg_4Al_{10}Si_2O_{23}$	–12 790 590.2	$S^0_{298.15} = 4\,S^0_{298.15}$ (MgO) + 5 $S^0_{298.15}$ (Al_2O_3) + 2 $S^0_{298.15}$ (SiO_2, tridymite) $C_P = 4\,C_P$(MgO) + 5 C_P(Al_2O_3) + 2 C_P(SiO_2, tridymite)

Data for all other compounds were taken from Wu et al.[9] and Eriksson et al.[10]

Liquid Oxide: CaO-MgO-$AlO_{1.5}$ and MgO-$AlO_{1.5}$-SiO_2

$\Delta g^0_{MgO,AlO_{1.5}} = -31\,518.04$

$q^{03}_{MgO,AlO_{1.5}} = -225\,764.46 + 66.72T$

$q^{06}_{MgO,AlO_{1.5}} = 80\,688.02$

$q^{07}_{MgO,AlO_{1.5}} = -48\,435.77$

$q^{001}_{MgO,AlO_{1.5}(SiO_2)} = 104\,600.0$

$q^{002}_{MgO,SiO_2(AlO_{1.5})} = 62\,395.99 - 52.30T$

$q^{001}_{AlO_{1.5},SiO_2(MgO)} = 250\,705.0 - 167.36T$

All other model parameters for binary systems were reported earlier.[9-11] The quasichemical parameters are defined in Ref. 7.

Monoxide: MgO-CaO-$AlO_{1.5}$

$G^0_{AlO_{1.5}} = 1/2G^0(\alpha - Al_2O_3) + 38\,702.0$

$q^{00}_{MgO,AlO_{1.5}} = 1\,548\,080 - 1347.68T + 0.286478T^2$

Parameters for the MgO-CaO subsystem were obtained previously.[9] The polynomial q parameters are defined in Ref. 12

Spinel: $(Mg^{2+}, Al^{3+})^T[Mg^{2+},Al^{3+},Va]^O_2O_4$

$G_{MA} = G^0(MgAl_2O_4)$:

$H^0_{298.15} = -2\,304\,994.88$

$S^0_{298.15} = 80.00$

$C_P = 795.470 - 0.33724T + 9.92769(10^{-5})T^2 + 79\,789.79T^{-1} - 761\,956.61T^{-2} - 14\,619.66T^{-0.5}$

$(15\ K < T < 3000\ K)$

G_{AA} is from Ref. 15

$\Delta_{MA:MA} = G_{AA} + G_{MM} - G_{MA} - G_{AM} = 40\,000.0$

$I_{MA} = G_{AA} + G_{AM} - 2G_{MA} = 21\,756.8 + 19.6648T$

$\Delta_{MA:MV} = G_{MM} + G_{AV} - G_{MV} - G_{AM} = -83\,680.00$

$G_{AV} = 8G^0(\gamma\text{-}Al_2O_3) - 2RT(5\ln 5\text{–}6\ln 6) - 5G_{AA}$, where

$G^o(\gamma\text{-}Al_2O_3) = G^o(\alpha\text{-}Al_2O_3) + 30\,000.0 - 12.500T$

Notations M, A, and V are used for Mg^{2+}, Al^{3+}, and vacancy, respectively.

Pyroxene: $(Mg)^{M2}(Mg^{2+},Al^{3+})^{M1}(Al^{3+},Si^{4+})^B(Si)^AO_6$

G_{MS} are from Ref. 18 for ortho-, proto-, and low clino-pyroxenes.

$G_{MS} + G_{AA} - G_{AS} - G_{MA} = 0.0$

$G_{AS} = G_{MA}$

$\Delta_{Mg\text{-}Ts} = (G^0_{CaMgSi_2O_6} + G_{AA}) - (G^0_{Mg_2Si_2O_6} + G^0_{CaAl_2SiO_6}) = 15\,899.2$

$L_{MA:A} = L_{MA:S}$ are from Ref. 20

Notations M, A, and S are used for Mg^{2+}, Al^{3+} and Si^{4+}, respectively.

$G^0_{CaMgSi_2O_6}$ and $G^0_{Mg_2Si_2O_2}$ are from previous study by Jung et al.[18]

$G^0_{CaAl_2SiO_6}$ is from F*A*C*T[19] database.

Note: Gibbs energies of the pure components of the solutions and of all binary stoichiometric components are taken from the F*A*C*T[19] database.

(where the notation M, A, and S indicates Mg^{2+}, Al^{3+}, and Si^{4+}, respectively).

The parameters G_{MS} are equal to $G^o(Mg_2Si_2O_6)$, the Gibbs energies of stable $Mg_2Si_2O_6$ enstatite (ortho-, proto-, and low clino-). These were evaluated previously.[18] For all polymorphs it was assumed that the Gibbs energy of the site exchange reaction is zero: $(G_{MS} + G_{AA}) - (G_{AS} + G_{MA}) = 0$. Furthermore, with no loss of generality, one can set $G_{AS} = G_{MA}$.

The parameter G_{AA} is equal to the Gibbs energy $G^o(MgAl_2SiO_6)$ of Mg-Tschermak which is not stable at 1.0 bar pressure, and for which no thermodynamic data exist. This was evaluated, for each polymorph, through the Gibbs energy $\Delta_{Mg\text{-}Ts}$ of the exchange reaction:

$$\Delta_{Mg\text{–}Ts} = (G^o_{CaMgSi_2O_6} + G^o_{MgAl_2SiO_6}) - (G^o_{Mg_2Si_2O_6} + G^o_{CaAl_2SiO_6}) \quad \text{(Eq 6)}$$

where the Gibbs energies of $CaMgSi_2O_6$, $Mg_2Si_2O_6$, and $CaAl_2SiO_6$, for all polymorphs are taken from previous optimizations.[18,19]

Finally, the G^E parameter $L_{M,A:A} = L_{M,A:S}$, which is related to interaction between Mg^{2+} and Al^{3+} on the M1 sites when the B sites are occupied by either Al^{3+} or Si^{4+}, was used. However, this parameter was not optimized in the current study, its value having already been fixed in an earlier study[15,20] to reproduce phase equilibrium and enthalpy of mixing data for $CaMgSi_2O_6$-$CaAl_2SiO_6$ (diopside-Ca-Tschermak) solutions.

2.3 Monoxide Solution

The MgO-CaO-$AlO_{1.5}$ monoxide solution was modeled as a simple random mixture of Mg^{2+}, Ca^{2+}, and Al^{3+} ions on cation sites with simple polynomial excess Gibbs energy terms.[12] It is assumed that cation vacancies remain associated with Al^{3+} ions and so do not contribute to the configurational entropy. Binary excess Gibbs energies were modeled by simple polynomial expansions in the mole fractions. Optimized parameters for the MgO-CaO binary system were obtained previously.[9] These model parameters reproduce the solid-solid miscibility gap in the MgO-CaO system. Additional parameters were optimized in the current study as described in the following sections. These are listed in Table 1. The properties of the ternary MgO-CaO-$AlO_{1.5}$ solution were calculated by means of the symmetric "Kohler-like" approximation.[12]

3. Thermodynamic Evaluations and Optimizations

3.1 MgO-Al_2O_3 System

3.1.1 Summary of Available Experimental Data. The phase diagram of the MgO-Al_2O_3 system is shown in Fig. 1. In a preliminary study, Rankin and Merwin[21] determined the congruent melting temperature of $MgAl_2O_4$. Alper et al.[22] determined the phase diagram of the MgO-$MgAl_2O_3$ system using a quenching technique followed by x-ray diffraction (XRD) or optical phase identification. Viechnicki et al.[23] investigated the solidus and liquidus under Ar atmospheres using the collapsing cone technique. They reported a eutectic reaction between spinel and Al_2O_3 at 1975 °C, which is higher than the temperature of 1925 °C reported by Rankin and Merwin.[21]

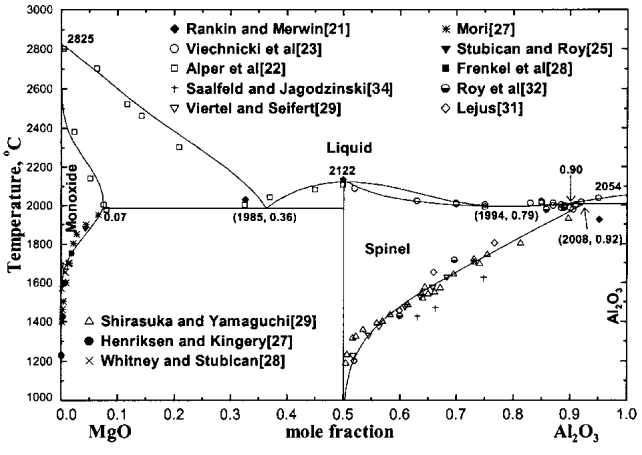

Fig. 1 Calculated phase diagram of the MgO-Al_2O_3 binary system

Many investigations have been performed to measure the solubility of Al_2O_3 in MgO (periclase)[22,24-28] and in the spinel solution[21,29-34] in the temperature range between 1230° and 1975 °C. Usually the solubilities were determined from the change of lattice parameters of quenched samples as determined by XRD. While the measured solubilities of Al_2O_3 in periclase show good agreement among authors, there is more scatter in the reported solubilities of Al_2O_3 in the spinel phase. Shirasuka and Yamaguchi[33] measured the solubility at temperatures between 1327 and 1927 °C. Viertel and Seifert[29] measured the solubility, seemingly with good accuracy, at 1 kbar total pressure in the temperature range between 1125 and 1625 °C using an equilibrium exsolution and homogenization technique.

According to Lejus and Collongues[35] and Lejus,[31] MgO is nearly insoluble in $MgAl_2O_4$. On the other hand, Alper et al.,[22] Chiang and Kingery,[36] and Fujii et al.[37] reported a low solubility (less than 3 mol%) of MgO in $MgAl_2O_4$. In general, solubility of MO in MAl_2O_4 spinels is rarely observed. The solubility of MgO in $MgAl_2O_4$ spinel was assumed to be negligible in the current study. Roy and Coble[38] reported a solubility of MgO in Al_2O_3 of about 0.1 mol% at 1830 °C and Ando and Momoda[39] reported a solubility of 0.012 mol%. The solubility of MgO in Al_2O_3 was assumed to be negligible in the current study.

The thermodynamic and structural properties of $MgAl_2O_4$ have been measured with good accuracy. The low temperature heat capacity of $MgAl_2O_4$ was measured by King[40] using adiabatic calorimetry, and its entropy at 298.16 K was determined. Heat contents of $MgAl_2O_4$ were measured by Bonnickson,[41] Landa and Naumova,[42] and Richet and Fiquet[43] at temperatures from 400-2200 K. The measured values are in good agreement with each other. The enthalpy of formation of $MgAl_2O_4$ from MgO and Al_2O_3 was measured at temperatures from 970-1173 K using calorimetric techniques.[44-46]

Gibbs energies of formation of $MgAl_2O_4$ from MgO and Al_2O_3 were measured by several authors[37,47-50] using different techniques. Taylor and Schmalzried,[49] and more recently Jacob and Jayadevan,[47] used a MgF_2 electrolyte to measure the Gibbs energy of $MgAl_2O_4$. Chamberlin et al.[48] equilibrated spinel and liquid Pd and measured the Mg and Al contents in the Pd. The oxygen partial pressure (controlled by H_2/CO_2 mixtures) was measured using a solid electrolyte. From the known activity coefficients of Mg and Al in the Pd alloy, the Gibbs energy of $MgAl_2O_4$ could thereby be calculated. Fujii et al.[37] performed similar measurements using liquid Cu. Rosen and Muan[50] equilibrated CoO-MgO and $CoAl_2O_4$-$MgAl_2O_4$ solid solutions under controlled P_{O_2}. From the known activities of CoO and MgO in the CoO-MgO solution (a nearly ideal solution) and the known Gibbs energy of $CoAl_2O_4$, the Gibbs energy of

$MgAl_2O_4$ could be estimated using a Gibbs-Duhem integration technique.

Grjøtheim et al.[51] measured the equilibrium partial pressure of Mg vapor over the three-phase mixture [MgO + $MgAl_2O_4$ + liquid Al] between 1143 and 1414 K. Altman[52] and Sasamoto et al.[53] measured the partial pressure of Mg over MgO and over $MgO{\cdot}xAl_2O_3$ spinel solutions (x = 1.0, 2.0, and 2.8) for the congruent vaporization of MgO (to Mg + 1/2 O_2 in vacuo) using a mass spectrometric/Knudsen-cell technique at temperatures between 1850 and 2300 K.

Navrotsky et al.[30] measured the enthalpy of formation of spinel solutions containing excess γ-alumina at 975 K using $2PbO{\cdot}B_2O_3$ solution calorimetry. McHale et al.[54] reinvestigated the enthalpy of transformation from α-Al_2O_3 (corundum) to γ-Al_2O_3 by calorimetric measurements on nanosized γ-Al_2O_3 with a correction being made for surface energy.

The cation distribution in spinel was measured for in situ or quenched samples by several authors[55-61] using several different techniques: XRD, neutron powder diffraction, NMR, ESR, etc. Redfern et al.[57] measured the cation distribution using an in situ neutron diffraction technique. They also examined the effect of nonstoichiometry of the spinel on the cation distribution. Navrotsky et al.[62] measured the enthalpy change for cation redistribution from 1200-973 K.

3.1.2 Evaluation and Optimization. Figure 1 shows the calculated optimized phase diagram of the MgO-Al_2O_3 binary system. All phase diagram data are reproduced within experimental error limits. The Al_2O_3 solubilities in spinel were optimized based mainly on the studies of Shirasuka and Yamaguchi[33] and Viertel and Seifert.[29]

At 25 °C, $MgAl_2O_4$ is a fully normal spinel. At higher temperatures, however, a significant degree of inversion occurs as can be seen in Fig. 2. The calculated optimized cation distribution is based mainly on the data of Redfern et al.[57] who appears to have taken care with sample preparation and experimental technique. The calculated cation distribution depends mainly on the optimized parameter I_{MA}.

In the experiments, the cation distribution becomes frozen in as the samples are cooled below $T_{frozen} \approx 973$ K, this temperature being estimated from the results of Redfern et al.[57] as seen in Fig. 2. Furthermore, above a temperature of $T_{unquen} \approx 1200$ K, the high temperature cation distribution cannot be retained by quenching, this temperature being estimated very roughly from the results of Wood et al.,[59] which appear to level off above this temperature. Hence, above ~1200 K the cation distribution can only be determined by in situ measurements.

Redfern et al.[57] also investigated the influence of the nonstoichiometry of spinel on the cation distribution and found that the degree of inversion increases with increasing Al_2O_3 dissolution. This possibly explains the scatter in the results of Peterson et al.,[56] whose samples had lower lattice parameters than the samples in other studies. Andreozzi et al.[61] recently measured the cation distribution using XRD. However, this technique is not sensitive because there is very little scattering contrast between Mg and Al.[57] In agreement with the results of Redfern et al., the degree of inversion was calculated to increase with increasing dissolution of Al_2O_3.

Calculated optimized thermodynamic properties of $MgAl_2O_4$ are shown in Fig. 3-8. As can be seen in Fig. 3, the calculated heat capacity is in good agreement with experimental data. The optimized entropy at 298.15 K is 80.14 J/mol · K which agrees well with the experimental value of 80.58 ± 0.5 J/mol · K of King.[40] $S^0_{298.15}$ of pure normal spinel in Table 1 is 80.00 J/mol · K. The difference is due to the slight degree of inversion at 298.15 K. The heat content measurements in Fig. 4 were obtained experimentally by quenching samples from a temperature T to 298.15 K. As discussed above, it is assumed that the cation distribution becomes frozen at its value at $T_{frozen} \approx 973$ K when a sample is quenched below this temperature, and that the cation distribution cannot be retained when quenched from temperatures above $T_{unquen} \approx 1200$ K. Therefore, the actual measured enthalpy difference in the quenching experiments, ΔH_{meas}, is assumed to be equal to:

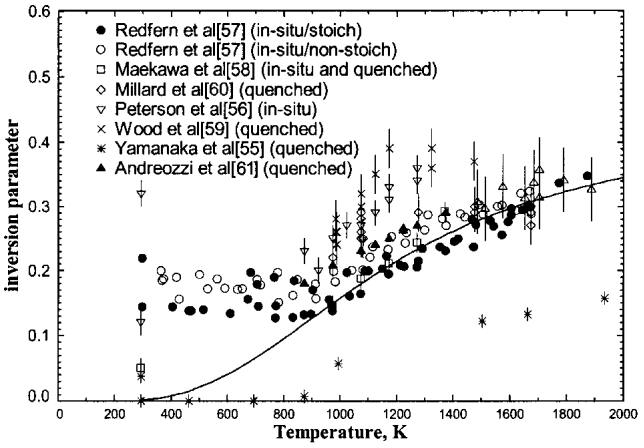

Fig. 2 Calculated variation of cation distribution in $MgAl_2O_4$. The inversion parameter is defined as the mole fraction of Al^{3+} on tetrahedral sites.

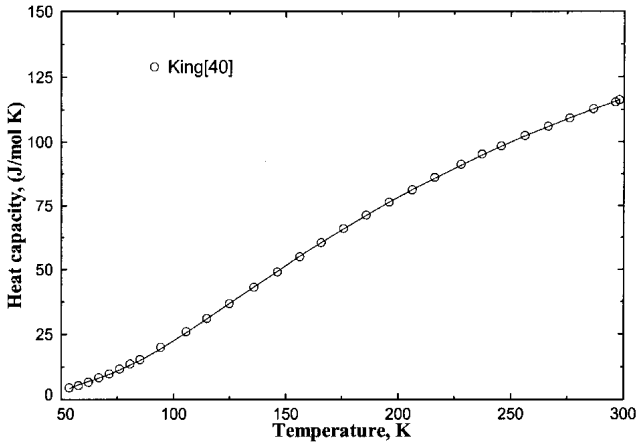

Fig. 3 Calculated heat capacity of $MgAl_2O_4$

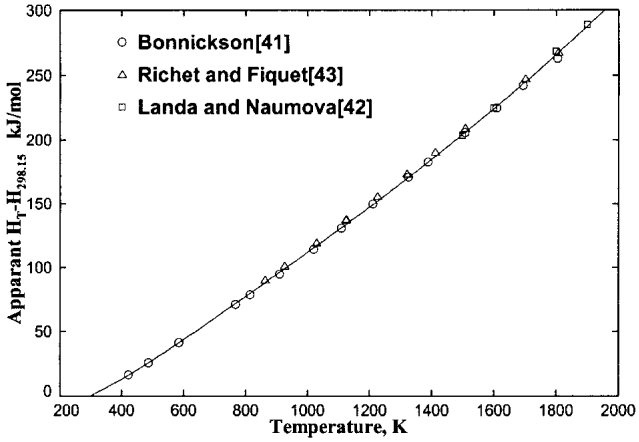

Fig. 4 Apparent heat content (H_T-$H_{298.15}$) of $MgAl_2O_4$ as reported in three studies. Line is calculated from the optimized model parameters with correction made for nonequilibrium cation distribution during the experiments (see text for details).

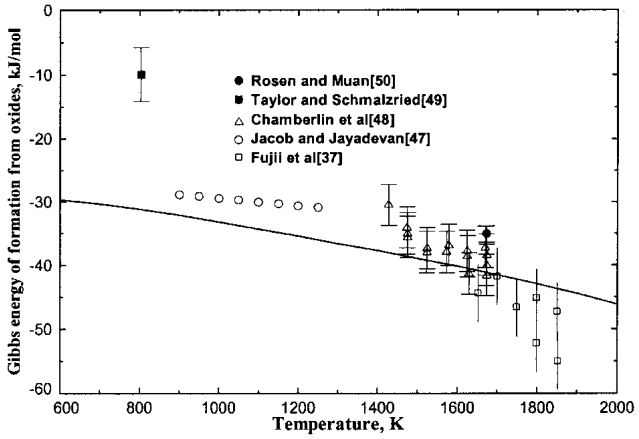

Fig. 5 Calculated Gibbs energy of formation for $MgAl_2O_4$ from solid MgO and Al_2O_3

$$T < 973: \quad \Delta H_{meas} = H_T \text{ (c.d. at 973)} - H_{298.15} \text{ (c.d. at 973)} \quad \text{(Eq 7)}$$

$$973 < T < 1200: \quad \Delta H_{meas} = H_T \text{ (c.d. at } T) - H_{298.15} \text{ (c.d. at } T) \quad \text{(Eq 8)}$$

$$T > 1200: \quad \Delta H_{meas} = H_T \text{ (c.d. at } T) - H_{298.15} \text{ (c.d. at 1200)} \quad \text{(Eq 9)}$$

where $H_{T'}$ (c.d. at T'') is the enthalpy at T' of a sample having the equilibrium cation distribution of a sample at T''. This correction to the reported heat contents is of the order of a few kJ/mol. With this correction, the measured and calculated heat contents are in excellent agreement as can be seen in Fig. 4.

Navrotsky[62] measured the annealing enthalpy for cation redistribution from 1200-973 K with the assumption that the heat capacity is independent of cation distribution. The calculated value of 1.9 kJ/mol agrees reasonably with the value of 1.1 ± 0.7 kJ/mol reported by Navrotsky.

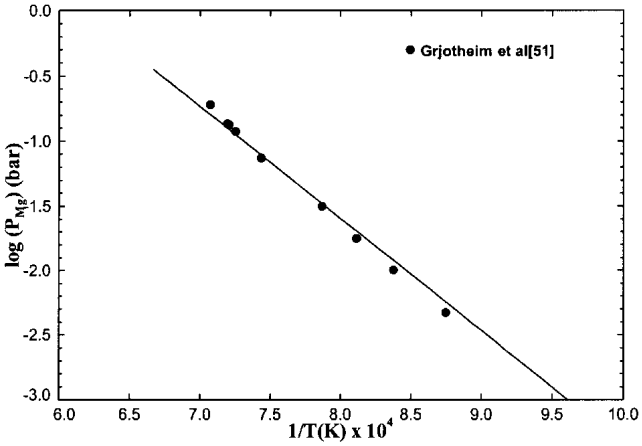

Fig. 6 Calculated partial pressure of Mg (gas) at equilibrium with (MgO + liquid Al alloy + $MgAl_2O_4$)

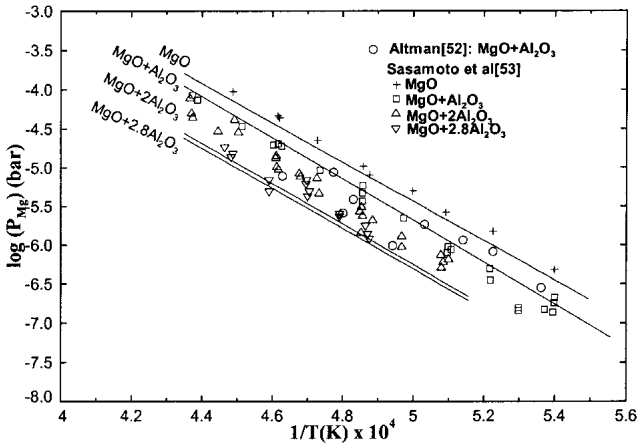

Fig. 7 Calculated partial pressure of Mg (gas) over MgO and over the spinel solid solution (MgO+xAl_2O_3) for congruent vaporization of MgO (to Mg(g) + 1/2O_2 in vacuo)

The enthalpy of formation of $MgAl_2O_4$ from MgO and Al_2O_3 was calculated as −22.7 kJ/mole at 970 K and −21.8 kJ/mole at 1173 K, in good agreement with the experimental data[44-46] (−24.7 or −22.5 ± 2.5 kJ/mol at 970 K, and −22.3 ± 2.8 kJ/mol at 1173 K). The value initially reported by Navrotsky and Kleppa[46] was revised by Schearer and Kleppa[45] using a more recent value of the enthalpy of dissolution of MgO in $PbO{\cdot}B_2O_3$. This revised value was used in the optimization in the current study.

The calculated Gibbs energy of formation of $MgAl_2O_4$ from solid MgO and Al_2O_3 is compared with experimental data in Fig. 5. The data of Taylor and Schmalzried[49] are not in agreement with the data of other authors. Also it was difficult to reproduce the measurements of Jacob and Jayadevan[47] who used emf cells with MgF_2 electrolytes as did Taylor and Schmalzried.

The calculated partial pressure of Mg(gas) at equilibrium with (MgO + liquid alloy + $MgAl_2O_4$) compares well with

the measurements[63] as shown in Fig. 6. The F*A*C*T*[19] database was used for the properties of Mg(gas) and for the activity of Mg in molten Al-Mg alloys. The calculated equilibrium solubility of Mg in the molten Al also agrees well with the reported[63] solubilities.

Figure 7 compares the calculated and experimental[52,53] equilibrium pressure of Mg(gas) for the congruent vaporization of MgO (to Mg(g) + 1/2 O_2 in vacuo) from MgO and from MgO·$x$$Al_2O_3$ spinel solutions (x = 1.0, 2.0, and 2.8) at various temperatures. The data are reproduced within the experimental error limits.

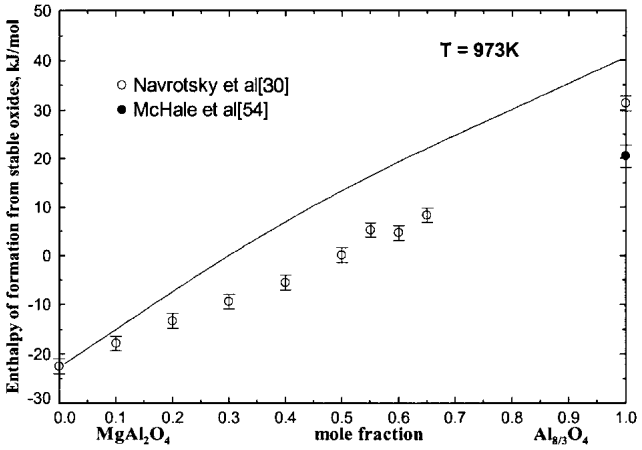

Fig. 8 Calculated enthalpy of formation of the spinel solution from MgO and α-Al_2O_3 at 973 K

The enthalpy of formation of the spinel solution ($MgAl_2O_4$-γ-$Al_{8/3}O_4$) from MgO and α-$Al_{8/3}O_4$ is plotted in Fig. 8. At an alumina mole fraction of 1.0, this enthalpy corresponds to the enthalpy of transformation of 4/3 mol of α-Al_2O_3 to 4/3 moles of γ-Al_2O_3. The point of McHale et al.[54] was obtained for nanosized materials with a correction being made for surface energy. The optimized value of 40 kJ per mole of $Al_{8/3}O_4$ is larger than the reported value because the optimized value was chosen to reproduce solubility data of Al_2O_3 not just in $MgAl_2O_4$ but in several other spinel phases[15] in the Fe-Mg-Al-Cr-Co-Ni-Zn-O system ($CoAl_2O_4$, $NiAl_2O_4$, $FeAl_2O_4$, and $ZnAl_2O_4$) simultaneously. If the spinel/(spinel + Al_2O_3) phase boundary in Fig. 1 is extrapolated to a mole fraction of Al_2O_3 of 1.0, the resultant temperature is the equilibrium temperature for the transformation of α-Al_2O_3 to metastable pure γ-Al_2O_3. Since this temperature must be the same for all spinel system, similar extrapolations were made for Fe-, Co-, Ni-, and Zn-spinels, and an average temperature of 2400 K was determined. Taking the above value of 30 kJ per mole of Al_2O_3 for the transformation enthalpy, the entropy of transformation is then calculated as 30 000/2400 = 12.500 J/mol · K. These values are shown in Table 1.

3.2 CaO-MgO-Al_2O_3 System

3.2.1 Summary of Available Experimental Data. The liquidus surface of the CaO-MgO-Al_2O_3 system is shown in Fig. 9. Rankin and Merwin[21] measured the phase diagram using a classic quenching technique followed by micro-

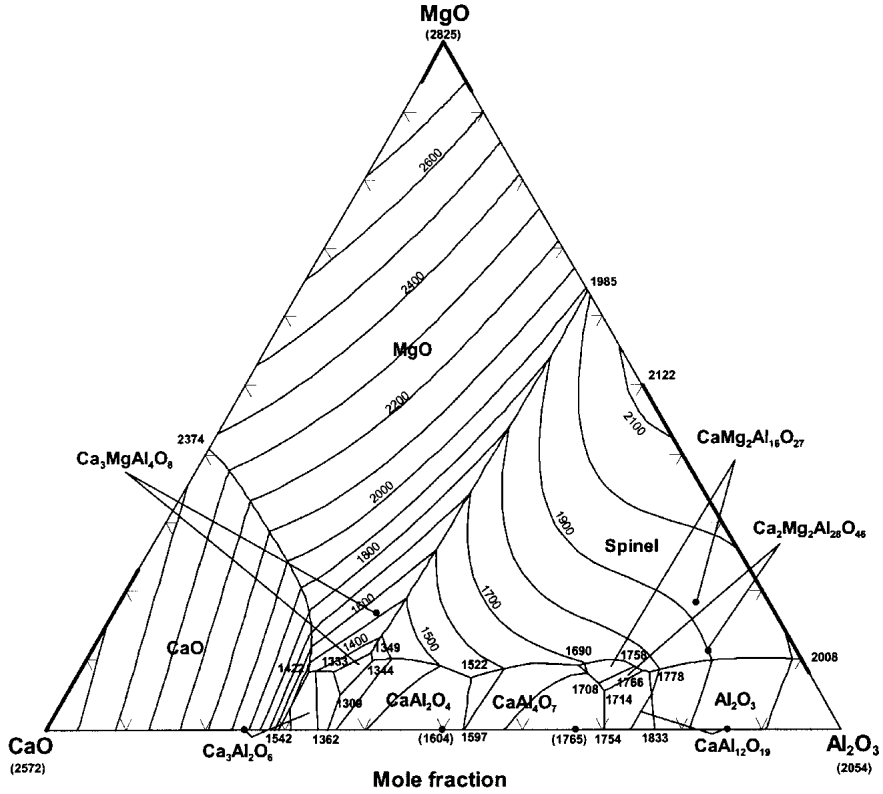

Fig. 9 Calculated liquidus projection of the CaO-MgO-Al_2O_3 system. Temperatures in °C

scopic primary phase determination. The $Ca_3MgAl_4O_8$ compound was first reported by Welch,[64] who also reported a metastable $Ca_7MgAl_{10}O_{23}$ ternary compound. Majumdar[65] investigated the primary crystallization region of the ternary $Ca_3MgAl_4O_8$ compound using XRD phase determination on quenched samples. Rao[66] determined phase diagrams of the $CaAl_2O_4$-$MgAl_2O_4$ and $CaAl_4O_7$-$MgAl_2O_4$ sections using hot stage microscopy. Melnik et al.[67] measured fusion temperatures in the $CaO{\cdot}Al_2O_3$-$MgAl_2O_4$-MgO section, but details of the experimental technique were not given and the measured data are ambiguous. Recently, De Aza et al.[68,69] investigated the phase diagram of the $CaO{\cdot}MgO$-Al_2O_3 section extensively using a quenching technique (air quenched at T < 1725 °C; quenched inside the furnace by switching off the power at T > 1725 °C) in the temperature range from 1350 to 2000 °C. The phases in the quenched samples were determined by XRD, and several compositions of the spinel solution were also measured by EPMA (WDS). This study reconfirmed the existence of the $CaMg_2Al_{16}O_{27}$ and $Ca_2Mg_2Al_{28}O_{46}$ phases originally reported by Göbbels et al.[70] and Iyi et al.,[71] and showed that these phases actually exist as solid solutions over very limited ranges of composition.[69-71] In the current study, these compounds were treated as stoichiometric. The liquidus isotherms at 1550, 1600, and 1650 °C were also measured by Ohta and Suito[72] and Hino et al.,[73] from analysis of slags at saturation in CaO, MgO, or Al_2O_3 crucibles.

Allibert et al.[74] measured the activities of CaO and MgO in molten slags at 1687 °C by a mass spectrometric/effusion cell technique. Activities of Al_2O_3 were then calculated from the Gibbs-Duhem equation. Hino et al.[73] equilibrated slags and liquid Cu at 1600 °C in carbon crucibles under a CO atmosphere and measured the Al, Ca, and Mg contents in the liquid Cu. From the known activity coefficients of Al, Ca, and Mg in liquid Cu, the activities of Al_2O_3, CaO, and MgO in the liquid slags were computed. Ohta and Suito[72] used a similar technique using liquid Fe at 1550 and 1600 °C and calculated activities in the molten slags saturated with CaO, MgO, or spinel.

3.2.2 Evaluation and Optimization. For the molten slag phase, no additional ternary model parameters were used; the properties of the ternary liquid were calculated entirely from the model parameters for the three binary subsystems using an asymmetric Toop-like approximation[12] with $AlO_{1.5}$ taken as the asymmetric component. The entropies and heat capacities of the ternary compounds $Ca_3MgAl_4O_8$, $CaMg_2Al_{16}O_{27}$, and $Ca_2Mg_2Al_{28}O_{46}$ were estimated as the weighted averages of the entropies and heat capacities of solid MgO, CaO, and Al_2O_3. The enthalpies of formation at 298.15 K were optimized in the current study to reproduce the phase equilibrium measurements. These are the only additional model parameters that were added in the optimization of the ternary system. The calculated liquidus projection is shown in Fig. 9.

The calculated primary crystallization fields in the CaO-MgO-Al_2O_3 system are plotted in Fig. 10 along with the experimental data of Rankin and Merwin,[21] Majumdar,[65] Rao,[66] and De Aza et al.[68,69] De Aza et al.[68,69] measured liquid compositions along the phase boundaries by EPMA (WDS) analysis of quenched samples. A $Ca_{12}Al_{14}O_{33}$ phase was observed by Rankin and Merwin and by Majumdar. However, it was concluded by Nurse et al.[75] that this compound is not stable in the anhydrous CaO-Al_2O_3 system but is only stabilized by the presence of moisture. Unstable $Ca_5Al_6O_{14}$, $Ca_3Al_{10}O_{18}$, and β-Al_2O_3 compounds were also observed by Rankin and Merwin. These compounds were not considered in the current study. The primary crystallization fields of $CaMg_2Al_{16}O_{27}$ and $Ca_2Mg_2Al_{28}O_{46}$ have not been investigated. Agreement between calculations and measurements is satisfactory as can be seen in Fig. 10.

Measured[21] and calculated liquidus temperatures are compared in Table 2. For the first listing in the table, the composition lies in the steepest part of the CaO liquidus (Fig. 9). On the second line in Table 2 it is shown that a composition change of only 0.7% decreases the calculated

Table 2 Comparison of Calculated Liquidus Temperature and Primary Solid Phase With Experimentally Determined Values[21] in the CaO-MgO-Al_2O_3 System

Composition, wt%				
CaO	MgO	Al_2O_3	Measured, °C	Calculated, °C
55	3	42	1525-1500, C	1617, C
(54.3)	(3)	(42.7)	…	(1530)
54	3	43	1490-1480, C3A	1487, C
48	4	48	1385-1378, C3A	1327, C3MA2
51	6	43	1450-1435, C3A	1506, M
35.2	2.8	62	1560-1550, CA	1543, CA
45	3	52	1395-1390, CA	1383, CA
42	5	53	1390-1360, CA	1381, CA
37	10	53	1525-1500, Sp	1490, Sp
34	12	54	1610-1575, Sp	1554, Sp
51.5	8	40.5	1540-1500, M	1710, C
45	8	47	1500-1450, M	1501, M
43	8	49	1500-1450, M	1459, M
40	10	50	1535-1510, M	1518, M

Note: Sp: Spinel, C*i*M*j*A*k* = *i*CaO·*j*MgO·*k*Al_2O_3

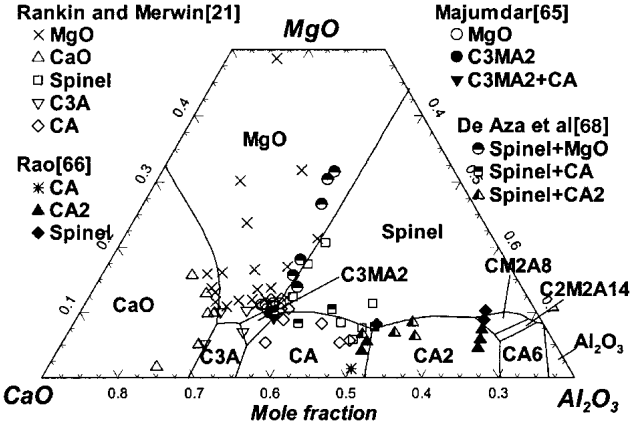

Fig. 10 Calculated primary crystallization fields of the CaO-MgO-Al_2O_3 system (C = CaO, A = Al_2O_3 and M = MgO)

liquidus temperature by 87 °C. The composition (eleventh line in Table 2), for which a temperature of 1710 °C is calculated, also lies in this region and very close to the boundary of the MgO crystallization field. In general, agreement in Table 2 is within experimental error limits. Calculated ternary invariant points are listed in Table 3 along with reported values. The values reported by De Aza et al.[69] are not shown because they were only estimated from widely spread experimental points.

Table 3 Comparison of Calculated Ternary Invariant Points With Experimental Results in the CaO-MgO-Al_2O_3 System

Equilibrium Solid Phases	Composition, mol % MgO	CaO	Al_2O_3	Temperature, °C
CaO + MgO + C3A: Per	8.2	62.9	28.9	1422 calc.
	10.3	61.8	27.9	1450 ± 5[21]
MgO + C3A + C3MA2: Per	8.3	59.7	32.0	1333 calc.
MgO + Sp + C3MA2: Per	11.1	53.6	35.3	1349 calc.
MgO + CA + C3MA2: Per	11.0	53.6	35.4	1350[65]
C3A + CA + C3MA2: Eu	4.9	60.6	34.5	1309 calc.
CA + Sp + C3MA2: Per	9.9	53.7	36.4	1344 calc.
CA + CA2 + Sp: Per	7.4	42.8	49.8	1522 calc.
CA2 + Sp + CM2A8: Per	9.2	28.4	62.4	1690 calc.
CA2 + CM2A8 + C2M2A14: Per	6.6	27.2	66.2	1708 calc.
CA2 + CA6 + C2M2A14: Per	5.5	27.0	67.5	1714 calc.
Sp + CM2A8 + C2M2A14: Per	9.0	21.5	69.5	1758 calc.
CA6 + Sp + C2M2A14: Per	8.4	20.8	70.8	1766 calc.
CA6 + Sp + Al_2O_3: Per	8.2	20.0	71.8	1778 calc.

Note: Sp: Spinel, C*i*M*j*A*k* = *i*CaO·*j*MgO·*k*Al_2O_3; Eu: Eutectic, Per: Peritectic reaction; calc.: calculated value from optimized phase diagram

Figure 11 shows the calculated $CaO{\cdot}MgO$-Al_2O_3 phase diagram section. Phase relations in this section were comprehensively measured by De Aza et al.[68,69] Since the samples were air quenched at $T < 1725$ °C and were quenched inside the furnace by switching off the power at $T > 1725$ °C, the quenching, especially from high temperatures, may have been too slow to assure that the equilibrium phase assemblages were retained. Solid phases could have precipitated during quenching. For example, $CaAl_{12}O_{19}$ is shown as stable up to 1875 °C, although the melting temperature of $CaAl_{12}O_{19}$ has been reported[11] to be about 1830 °C. Because liquidus temperatures are well predicted over a wide range of compositions in the ternary system (see Table 2), the inconsistency between De Aza et al.'s measurements and the calculations in Fig. 11 could be due to experimental errors caused by the quenching process. The enthalpies of the two ternary compounds, $CaMg_2Al_{16}O_{27}$ and $Ca_2Mg_2Al_{28}O_{46}$ were optimized assuming that reported temperatures in Fig. 11 are 30-50 °C too high. With this provision, the complex phase relations in the $CaO{\cdot}MgO$-Al_2O_3 section are satisfactorily reproduced.

Calculated liquidus isotherms of the CaO-MgO-Al_2O_3 system at 1550, 1600, and 1650 °C are compared with experimental data[72,73] in Fig. 12. Agreement is within experimental error limits.

The $CaAl_4O_7$-$MgAl_2O_4$ phase diagram section reported by Rao[66] is compared with calculations in Fig. 13. Agreement is not good. Hallstedt[3] observed similar disagreement with his calculations. However, the calculations are consistent with liquidus measurements of other authors in the same composition range. Also, as can be seen in Fig. 13, extrapolation of Rao's points to zero wt.% $MgAl_2O_4$ gives a liquidus temperature, which is much higher than that obtained in the earlier[11] evaluation of the CaO-Al_2O_3 binary system in which all available binary data were considered.

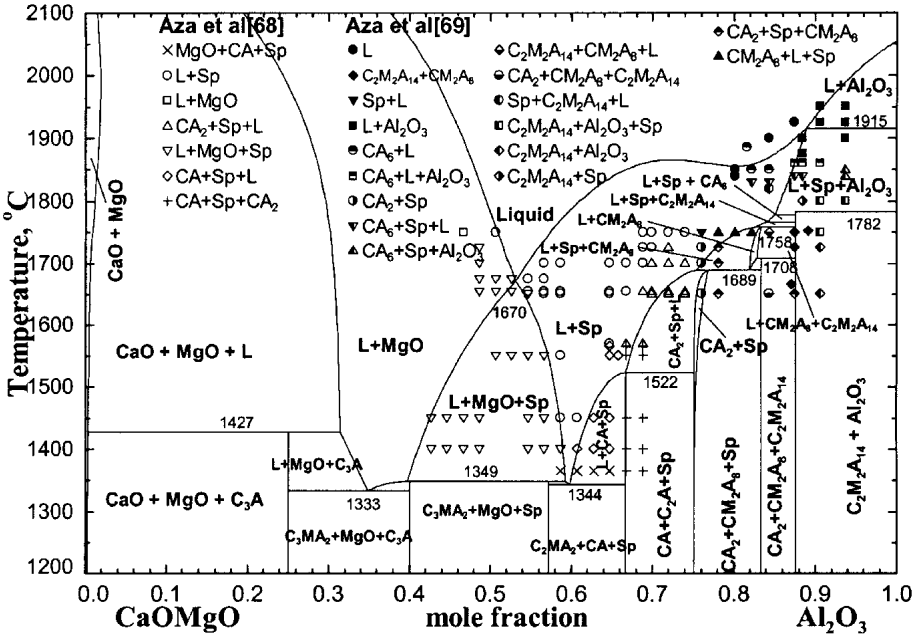

Fig. 11 Calculated phase diagram for the $CaMgO_2$-Al_2O_3 section (Sp = spinel, L = liquid, C = CaO, A = Al_2O_3 and M = MgO)

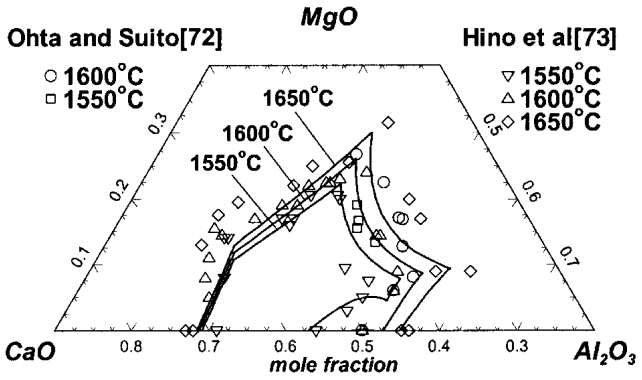

Fig. 12 Calculated liquidus of the CaO-MgO-Al_2O_3 system at 1550, 1600 and 1650 °C

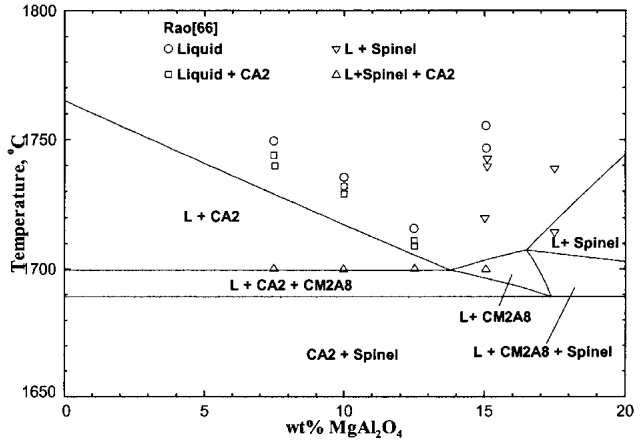

Fig. 13 Calculated phase diagram of the $CaAl_4O_7$-$MgAl_2O_4$ section (L = liquid, C = CaO, A = Al_2O_3 and M = MgO)

Similarly, the phase diagram measurements of Rao[66] in the $CaAl_2O_4$-$MgAl_2O_4$ section (up to 20 wt.% $MgAl_2O_4$) are not well reproduced unless it is assumed that excess Al_2O_3 was present in the experiments. This observation was also made by Hallstedt.[3]

Calculated iso-activity curves in CaO-MgO-Al_2O_3 liquid slags are shown in Fig. 14 and 15. The data of Ohta and Suito,[72] Hino et al.,[73] and Allibert et al.[74] are not in good agreement with the calculations. However, the disagreement among the different authors is as great as their disagreement with the calculations. The activities of CaO reported by Ohta and Suito were calculated from the measured equilibrium concentration of Ca in molten Fe in equilibrium with the slags. To calculate the activity of CaO, the activity coefficient of Ca in Fe was used. However, this activity coefficient is not well known and could be in serious error.

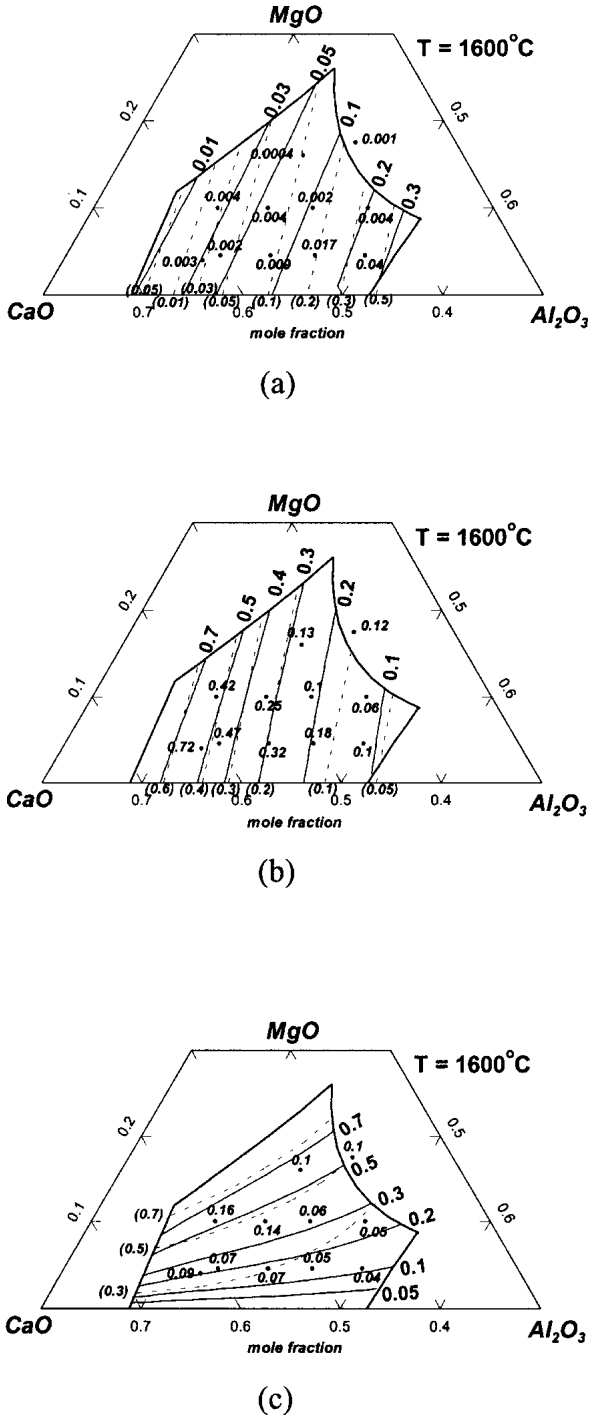

Fig. 14 Calculated activities in CaO-MgO-Al_2O_3 liquid slags at 1600 °C. **(a)** Al_2O_3 (solid standard state). **(b)** CaO (solid standard state). **(c)** MgO (solid standard state). Experimental points from Hino et al.[73] and dotted lines from Ohta and Suito.[72]

3.3 MgO-Al_2O_3-SiO_2 System

3.3.1 Summary of Available Experimental Data. The liquidus projection of the MgO-Al_2O_3-SiO_2 system is shown in Fig. 16. Greig[76] studied the liquid miscibility gap using a quenching technique. Rankin and Merwin[77] investigated the phase diagram mainly below 1550 °C using a classic quenching technique. They determined the primary phase regions of pyroxene, forsterite, spinel, Al_2O_3, SiO_2, and the ternary cordierite ($Mg_2Al_4Si_5O_{18}$) phase. The unstable sillimanite (Al_2SiO_5) phase was observed instead of

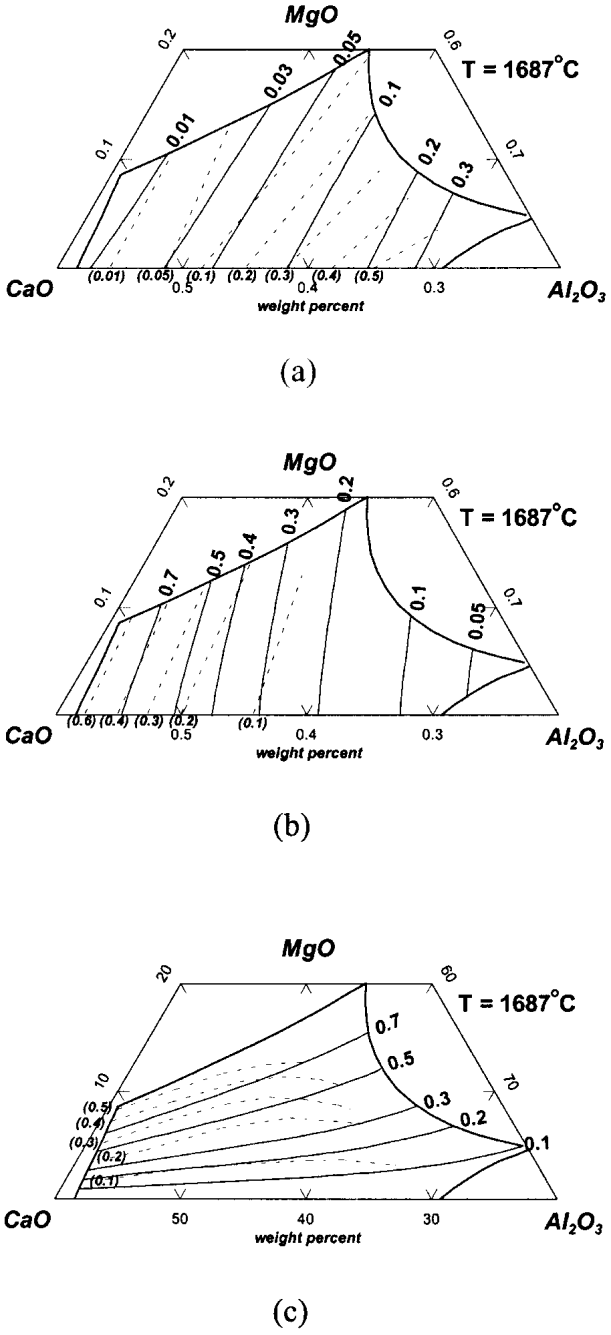

Fig. 15 Calculated activities in CaO-MgO-Al_2O_3 liquid slags at 1687 °C. **(a)** Al_2O_3 (solid standard state). **(b)** CaO (solid standard state). **(c)** MgO (solid standard state). Dotted lines from Allibert et al.[74]

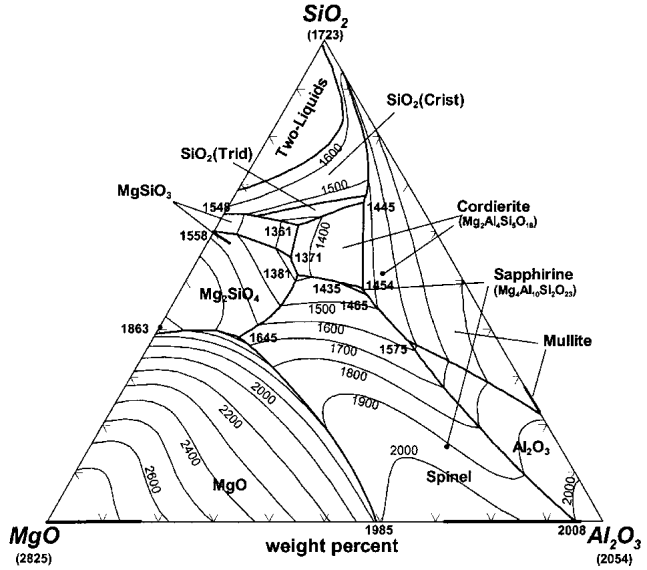

Fig. 16 Calculated liquidus surface of the MgO-Al_2O_3-SiO_2 system. Temperatures in °C

mullite at certain compositions. Later, Schreyer, and Schairer[78,79] comprehensively investigated the phase equilibria related to the ternary cordierite phase. Keith and Schairer[80] investigated the tiny stability field of sapphirine using a quenching technique. Aramaki and Roy[81] studied the phase boundary between mullite and corundum using a quenching technique with optical and XRD phase identification. Schlaudt and Roy[82] investigated the periclase (MgO) solid solution. Both Al_2O_3 and SiO_2 were reported to be soluble. However, in an earlier evaluation of the MgO-SiO_2 system[12] it was concluded that the solubility of SiO_2 in solid MgO is negligible. Onuma and Arita[83] investigated the solubilities of Al^{3+} in the $MgSiO_3$ pyroxene phase using a technique of quenching with optical and XRD phase analysis. They found that proto-enstatite ($MgSiO_3$) dissolves Mg-Tschermak $MgAl_2SiO_6$ up to about 6 wt.% at a pressure of 1 bar. Anastasiou and Seifert[84] measured the solubility of Al_2O_3 in ortho-enstatite at pressures of 1-5 kbar using a quenching technique, finding a nearly pressure-independent solubility of about 5 wt.% near 1000 °C.

Cordierite has two polymorphic forms. Low temperature cordierite has a completely ordered orthorhombic structure (*Cccm*). It transforms to the high temperature form with a hexagonal structure (*P6/mmc*) with long range ordering of Al and Si at about 1450 °C, before melting at 1460 °C. Cordierite exhibits a range of solid solution, dissolving up to approximately 20 wt.% of the theoretical compound Mg-beryl ($Mg_3A1_2SiO_{23}$).[77,79,85] Smart and Glasser[85] reported very complex phase equilibria involving the cordierite solid solution within a very narrow range of composition and temperature. The ternary sapphirine phase exhibits a very limited range of solid solution over the composition range $Mg_7Al_{22-x}Si_{0.75x}O_{40}$ ($1.5 < x < 5.6$).[85] These complexities of cordierite and sapphirine were not considered in the current study. For the sake of simplicity, only orthorhombic cordierite was considered, and it and sapphirine were taken to be stoichiometric ternary compounds. The formula of sapphirine was assumed to be $Mg_4Al_{10}Si_2O_{23}$ following Osborn and Muan[86] and Foster.[87]

Sub-solidus phase equilibria were investigated by several authors[85,87-89] using a sintering technique and x-ray phase determination. Smart and Glasser[89] and Foster[87] reported that the (sapphirine + corundum + mullite) phase assem-

blage transformed to (spinel + mullite + corundum) above about 1460 °C. Smart and Glasser[89] reported that the (sapphirine + cordierite + corundum) phase assemblage transformed to (sapphirine + cordierite + mullite) above about 1386 °C. Sakai and Kawasaki[88] found that the ($MgSiO_3$ + cordierite + spinel) phase assemblage transformed to (Mg_2SiO_4 + cordierite + spinel) at a temperature between 1000 and 1050 °C.

The thermodynamic properties of cordierite and sapphirine have been measured. Weller and Kelley[90] measured the heat capacity of stoichiometric ordered orthorhombic cordierite at low temperatures using adiabatic calorimetry. Geiger and Voigtlander[91] measured the heat capacity of cordierite from 330 to 950 K using differential scanning calorimetry (DSC). The heat content of stoichiometric cordierite was measured by Pankratz and Kelly[90] and Mueller et al.[92] using calorimetry. No heat capacity measurements for sapphirine ($Mg_4Al_{10}Si_2O_{23}$) have been reported. Carlu et al.[44] measured enthalpies of formation of $4MgO{\cdot}5Al_2O_3{\cdot}2SiO_2$ sapphirine and aluminous orthoenstatite, $(MgSiO_3)_{0.9}(Al_2O_3)_{0.1}$, from the oxides at 970 K using $2PbO{\cdot}B_2O_3$ solution calorimetry. Roy and Navrotsky[93] measured the enthalpy of MgO-Al_2O_3-SiO_2 glasses by $2PbO{\cdot}B_2O_3$ solution calorimetry at 970 K. Courtial and Richet[94] also measured the heat content of MgO-Al_2O_3-SiO_2 glasses. However, since both of these experiments investigated the enthalpy of glasses rather than of the molten slag, these data were not used in the present optimizations.

Rein and Chipman[95] investigated the activity of SiO_2 in ternary liquid slags using the equilibria between slags and Fe-Si-C alloys in graphite or SiC crucibles at 1600 °C under pure CO gas atmospheres. Henderson and Taylor[96] determined the activity of SiO_2 in liquid slags at 1500 °C and 1550 °C by measuring the equilibrium CO pressure for the equilibrium: $SiO_2 + C = SiC + 2CO$.

3.3.2 Evaluation and Optimization. In the present optimization, three additional ternary model parameters for the liquid slag (Table 1) and one additional model parameter $\Delta_{Mg\text{-}Ts}$ (Table 1) for the pyroxene solutions were required to reproduce the available data for the MgO-Al_2O_3-SiO_2 system.

The entropy and heat capacity of $Mg_2Al_4Si_5O_{18}$ cordierite (Table 1) were taken from Berman.[97] Its enthalpy of formation was altered by −9 kJ/mol from the value recommended by Berman to best reproduce the phase equilibrium data. The enthalpy of formation of $Mg_4Al_{10}Si_2O_{23}$ sapphirine shown in Table 1 was optimized to reproduce its reported primary crystallization field. Its entropy and heat

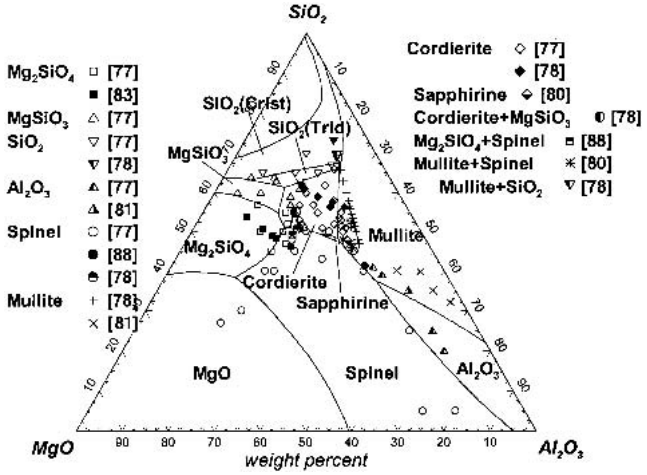

Fig. 17 Calculated liquidus surface of the MgO-Al_2O_3-SiO_2 system showing primary crystallization fields

Table 4 Comparison of Calculated Ternary Invariant Points With Experimental Results in the MgO-Al_2O_3-SiO_2 System

Equilibrium Solid Phases	Liquid Composition, wt.% MgO	Al_2O_3	SiO_2	Temperature, °C
Py + Tr + Cord: Eu	24.0	14.5	61.5	1361 calc.
	20.3	18.3	61.4	1345 ± 5[77]
	20.5	17.5	62	1356[78,79]
				1345 ± 2[89]
For + Py + Cord: Eu	28.5	16.7	54.8	1371 calc.
	25.0	21.0	54.0	1360 ± 5[77]
	24.87	20.22	54.91	1364 ± 2[78,79]
				1360 ± 2[89]
For + Sp + Cord: Per	29.3	19.6	51.1	1381 calc.
	25.7	22.8	51.5	1370 ± 5[77]
	24.9	23.0	52.1	1380[88]
				1373 ± 2[89]
Mull + Tr + Cord: Per	10.3	23.6	66.1	1445 calc.
(*Sil instead of Mull*)	10.0	23.5	66.5	1425 ± 5[77]
				1443 ± 5[80]
				1444 ± 2[89]
Sp + Sa + Cord: Per	22.4	27.9	49.6	1435 calc.
	17.4	33.5	49.1	1453 ± 5[80]
				1448 ± 2[89]
Sp + Mull + Sa: Per	19.0	33.7	47.3	1465 calc.
	16.9	36.8	46.3	1482 ± 3[80]
				1475[87]
				1469 ± 2[89]
Mull + Sa + Cord: Per	18.9	32.6	48.5	1454 calc.
	16.3	34.4	49.3	1460 ± 5[80]
				1454 ± 2[89]
Cor + Sp + Mull: Per	16.1	46.4	37.5	1575 calc.
				1560 ± 15[89]
For + Per + Sp: Per	46.4	15.1	38.5	1645 calc.
	56.0	16.0	28.0	1700 ± 25[80]
Tr + Cris + Py: Per	30.3	6.3	63.4	1465 calc.
Tr + Cris + Mull: Per	9.3	23.2	67.5	1465 calc.
Sil + Sp + Cord: Per	16.1	34.8	49.1	1460 ± 5[77]
Cor + Sp + Sil: Per	15.2	42.0	42.8	1575 ± 5[77]

Note: Tr: Tridymide (SiO_2), Crist: Cristobalite (SiO_2), Mu: Mullite ($Al_6Si_2O_{13}$), Cor: Corundum (Al_2O_3), Sp: Spinel solution, Py: Pyroxene solution, For: Forsterite (Mg_2SiO_4), Cord: Cordierite ($Mg_2Al_4Si_5O_{18}$), Sa: Sapphirine ($Mg_4Al_{10}Si_2O_{23}$), Sil: Sillimanite (Al_2SiO_5). (Sillimanite is unstable). Eu: Eutectic; Per: Peritectic reaction; calc.: calculated value from optimized phase diagram

capacity were estimated as the weighted averages of those of solid MgO, Al_2O_3, and SiO_2. The optimized enthalpy of formation of sapphirine from the oxides is −188.2 kJ/mol at 970 K, which may be compared with the reported −161.5 ± 5 kJ/mol.[44]

The calculated liquidus projection is shown in Fig. 16. The primary crystallization fields are plotted again in Fig. 17 along with data taken from several studies.[77-80,83,88,98] In general, the calculated cordierite phase field is displaced to the left (toward the MgO-SiO_2 side) relative to the measurements. This discrepancy can also be seen in Table 4 where the calculated invariant points are compared with reported values from several studies.[77-80,87-89] The calculated and reported invariant temperatures are generally in good agreement, but the calculated invariant liquid compo sitions are generally shifted by a few wt.% to higher MgO and lower Al_2O_3 contents relative to the measured compositions.

Table 5 Comparison of Calculated Liquidus Temperature and Primary Solid Phase With Experimentally Determined Values[77] in the MgO-Al_2O_3-SiO_2 System

Composition, wt.%				
MgO	Al_2O_3	SiO_2	Measured, °C	Calculated, °C
17.5	42.5	40	1583-1570, Sp	1553, Sp
29	23	48	1450-1430, Sp	1448, Sp
20	30	50	1450-1435, Sp	1449, Cord
25	25	50	1410-1390, Sp	1423, Sp
26	23	51	1380-1376, Sp	1407, Cord
35	20	45	1555-1550, For	1497, Sp
35	15	50	1560-1530, For	1485, For
26	21	53	1375-1365, For	1402, Cord
27	18	55	1415-1390, For	1385, Cord
25	20	55	1375-1365, Py	1402, Cord
24	17	59	1383-1370, Py	1385, Cord
35	5	60	1515-1510, Py	1489, Py
21	18	61	1370-1360, Py	1398, Cord
25	12	63	1440-1420, Py	1413, SiO_2
30	6	64	1500-1498, Py	1488, SiO_2
25	11	64	1450-1425, Py	1446, SiO_2
20	15	65	1455-1450, SiO_2	1449, SiO_2
11	22	67	1455-1435 SiO_2	1461, SiO_2
20	18	62	1355-1352, SiO_2	1399, Cord
15	15	70	1530-1500, SiO_2	1538, SiO_2
16	34	50	1460-1457, Cord	1503, Mull
20	23	57	1400-1375, Cord	1434, Cord
18	30	52	1450-1425, Cord	1458, Cord
25	23	52	1370-1365 Cord	1413, Cord
20	25	55	1415-1400, Cord	1441, Cord
15	30	55	1460-1450, Cord	1470, Mull
23	20	57	1375-1350, Cord	1409, Cord
15	27	58	1450-1425, Cord	1458, Cord
20	20	60	1365-1340, Cord	1416, Cord
15	23	62	1425-1400, Cord	1443, Cord
11	23	66	1450-1440, Cord	1445, SiO_2

Note: Sp: Spinel; For: Forsterite (Mg_2SiO_4); Py: Pyroxene ($MgSiO_3$ solution); Cord: Cordierite ($Mg_2Al_4Si_5O_{18}$); Mull: Mullite

In Fig. 17, it is seen that Rankin and Merwin[77] observed spinel as the primary phase at two compositions where the calculations predict MgO. However, small amounts of MgO and $MgAl_2O_4$ embedded in a glassy phase are difficult to distinguish by optical microscopy.[99] The calculated liquid miscibility gap extends to 11.5 wt.% Al_2O_3 at 1615 °C. Greig[76] reported that the liquid miscibility gap extends to 5 wt.% Al_2O_3 at 1600 °C. Such a rapid disappearance of the miscibility gap with small additions of Al_2O_3 is surprising and is very difficult to reproduce with the slag model. On the other hand, the measurements in viscous high-SiO_2 slags are very difficult.

Calculated and measured liquidus temperatures are compared in Table 5. Agreement with the data of Rankin and Merwin[77] (from 1918) is reasonable.

The calculated phase diagrams for the cordierite-SiO_2, cordierite-$MgAl_2O_4$, and $MgSiO_3$-$MgAl_2SiO_6$ sections are presented in Fig. 18-20. The calculated diagrams agree with the experimental data[78,79,83] within the experimental error limits. The enthalpy of formation of aluminous ortho-

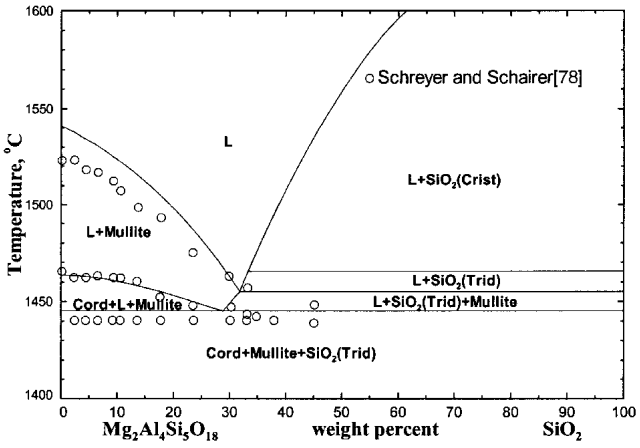

Fig. 18 Calculated phase diagram for the $Mg_2Al_4Si_5O_{18}$ (cordierite)-SiO_2 section

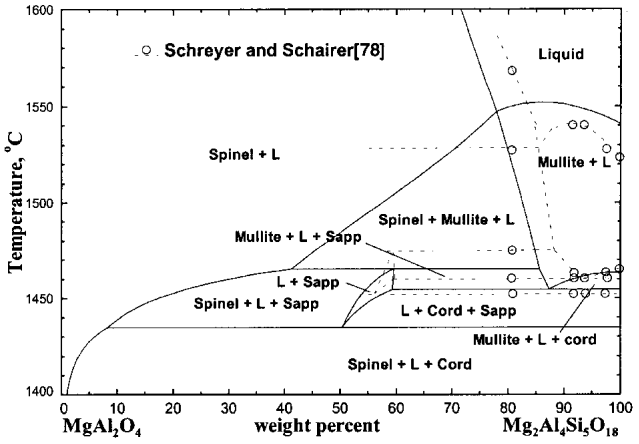

Fig. 19 Calculated phase diagram for the $MgAl_2O_4$-$Mg_2Al_4Si_5O_{18}$ (cordierite) section. Dotted lines indicate diagram proposed by Schreyer and Schairer.[78,79]

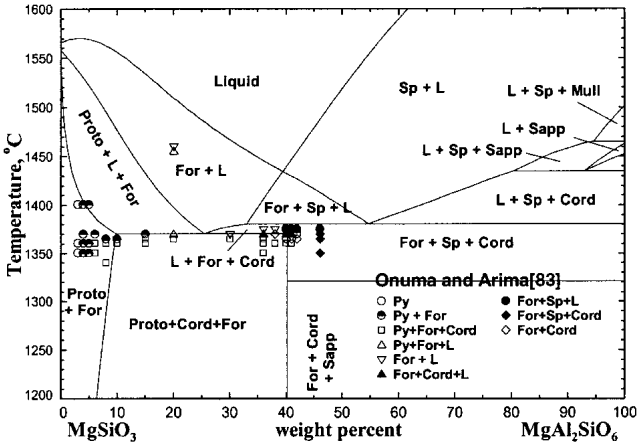

Fig. 20 Calculated phase diagram for the $MgSiO_3$-$MgAl_2SiO_6$ section. (For: forsterite, Sp: Spinel, Proto: proto-pyroxene, Cord: cordierite, Sapp: sapphirine, L: liquid, and Mull: mullite)

enstatite, $(MgSiO_3)_{0.9}(Al_2O_3)_{0.1}$, from solid MgO, SiO_2, and Al_2O_3 is calculated as −22.5 kJ/mole at 970 K, which may be compared with the value of −29.3 ± 0.6 kJ/mol measured by Charlu et al.[44]

It was difficult to reproduce the subsolidus phase equilibria in this study. The phase assemblage of (sapphirine + corundum + mullite) is calculated to transform to (spinel + mullite + corundum) at 1366 °C, which is almost 100 °C lower than the reported temperature[85,87] The reported three-phase fields of (sapphirine + cordierite + corundum)[89] and ($MgSiO_3$ + cordierite + spinel)[88] are never calculated to be stable. This discrepancy may be partially due to the fact that solid solubility in cordierite and sapphirine was ignored in the current study.

Figure 21 shows calculated activities of SiO_2 (solid cristobalite standard state) in MgO-Al_2O_3-SiO_2 liquid slags at 1500, 1550, and 1600 °C along with reported values. The discrepancy between the two experimental studies is evident. The calculated activities are closer to the results of Henderson and Taylor.[96]

In general, the difficulties encountered during optimization of the MgO-Al_2O_3-SiO_2 system were greater than with most other oxide systems that the authors have evaluated/optimized. Some of the remaining discrepancies may be due to their ignoring solid solubility in cordierite and sapphirine. On the other hand, there have been no extensive phase diagram studies since 1918.[77]

4. Conclusions

A complete critical evaluation of all available phase diagram and thermodynamic data for the MgO-Al_2O_3, CaO-MgO-Al_2O_3, and MgO-Al_2O_3-SiO_2 systems has been carried out, and a database of optimized model parameters has been developed. A wide variety of available data are reproduced within experimental error limits by a very few model parameters. With the present optimized database, it is possible to calculate any phase dia-

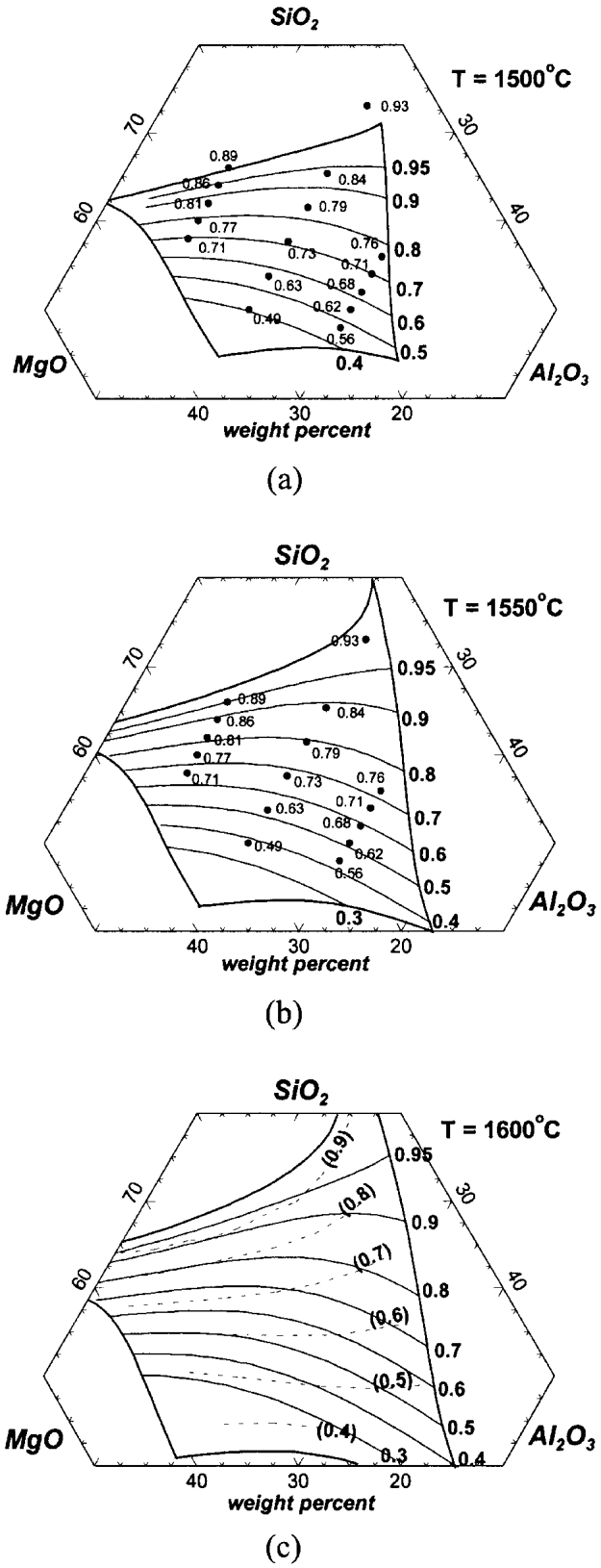

Fig. 21 Calculated activities of SiO_2 (solid cristobalite standard state) in MgO-Al_2O_3-SiO_2 liquid slags. **(a)** 1500 °C. **(b)** 1550 °C. **(c)** 1600 °C. Experimental points (a) and (b) from Henderson and Taylor[96] and dotted lines (c) from Rein and Chipman.[95]

gram section for all compositions. The optimized parameters form part of the F*A*C*T* database and can be used together with the FactSage[19] software for thermodynamic modeling of various industrial and natural processes.

Acknowledgments

This project was supported by a CRD grant from the Natural Sciences and Engineering Research Council of Canada in collaboration with INCO, Noranda, Rio Tinto, Teck Cominco, Alcoa, Dupont, Shell, Corning, Pechiney, Norsk Hydro, Sintef, Schott Glas, St.-Gobain Recherche, Mintek and IIS Materials.

References

1. G. Eriksson, P. Wu, and A.D. Pelton: "Critical Evaluation and Optimization of the Thermodynamic Properties and Phase Diagrams of the Magnesia-Alumina, Manganese(II) Oxide-Al_2O_3, Ferrous Oxide-Al_2O_3, Sodium Oxide-Al_2O_3, and Potassium Oxide-Al_2O_3 Systems," *Calphad,* 1993, *17,* pp. 189-205.
2. B. Hallstedt: "Thermodynamic Assessment of the System MgO-Al_2O_3," *J. Am. Ceram. Soc.,* 1992, *75,* pp. 1497-1507.
3. B. Hallstedt: "Thermodynamic Assessment of the CaO-MgO-Al_2O_3 System," *J. Am. Ceram. Soc.,* 1995, *78*, pp. 193-98.
4. S.A. Decterov, E. Jak, P.C. Hayes, and A.D. Pelton: "Experimental Study of Phase Equilibria and Thermodynamic Optimization of the Fe-Zn-O System," *Metall. Mater. Trans. B.,* 2001, *32 B,* pp. 643-57.
5. A.D. Pelton and M. Blander: "Computer-Assisted Analysis of the Thermodynamic Properties and Phase Diagrams of Slags" in *Proceedings of the Second International Symposium on Metallurgical Slags and Fluxes,* TMS-AIME, Warrendale, PA, 1984.
6. A.D. Pelton and M. Blander: "Thermodynamic Analysis of Ordered Liquid Solutions by a Modified Quasi-Chemical Approach. Application to Silicate Slags," *Metall. Trans. B,* 1986, *17B,* pp. 805-15.
7. A.D. Pelton, S.A. Decterov, G. Eriksson, C. Robelin, and Y. Dessureault: "The Modified Quasichemical Model. I—Binary Solutions," *Metall. Mater. Trans. B,* 2000, *31B,* pp. 651-59.
8. A.D. Pelton and P. Chartrand: "The Modified Quasichemical Model. II—Multicomponent Solutions," *Metall. Mater. Trans. A,* 2001, *32A,* pp. 1355-60.
9. P. Wu, G. Eriksson, and A.D. Pelton: "Critical Evaluation and Optimization of the Thermodynamic Properties and Phase Diagrams of the Calcia-Iron(II) Oxide, Calcia-Magnesia, Calcia-Manganese(II) Oxide, Iron(II) Oxide-Magnesia, Iron(II) Oxide-Manganese(II) Oxide, and Magnesia-Manganese(II) Oxide Systems," *J. Am. Ceram. Soc.,* 1993, *76,* pp. 2065-75.
10. G. Eriksson and A.D. Pelton: "Critical Evaluation and Optimization of the Thermodynamic Properties and Phase Diagrams of the CaO-Al_2O_3, Al_2O_3-SiO_2, and CaO-Al_2O_3-SiO_2 Systems," *Metall. Trans.,* 1993, *24B,* pp. 807-16.
11. P. Wu, G. Eriksson, A.D. Pelton, and M. Blander: "Prediction of the Thermodynamic Properties and Phase Diagrams of Silicate Systems: Evaluation of the FeO-MgO-SiO_2 System," *ISIJ Inter.,* 1993, *33,* pp. 26-35.
12. A.D. Pelton: "A General 'Geometric' Thermodynamic Model for Multicomponent Solutions," *Calphad,* 2001, *25,* pp. 319-28.
13. M. Hillert, B. Jansson, and B. Sundman: "Application of the Compound-Energy Model to Oxide Systems," *Z. Metallkd.,* 1988, *79,* pp. 81-87.
14. H.S.C. O'Neill and A. Navrotsky: "Cation Distributions and Thermodynamic Properties of Binary Spinel Solid Solutions," *Am. Mineral.,* 1984, *69,* pp. 733-53.
15. S.A. Decterov, I.-H. Jung, Y.-B. Kang, E. Jak, V. Swamy, D. Kevorkov, and A.D. Pelton: "Report for Oxide Database Development," CRCT, Ecole Polytechnique, Montreal, 2002.
16. N. Morimoto: "Nomenclature of Pyroxenes," *Mineral. Mag.,* 1988, *52,* pp. 535-50.
17. P. Shi, S.K. Saxena, Z. Zang, and B. Sundman: "Thermodynamics of the Ca-Mg-Fe-Al-Si-O Pyroxenes: 1. Theoretical Model and Assessment of the Ca-Mg-Si-O System," *Calphad,* 1994, *18,* pp. 47-69.
18. I.-H. Jung, S.A. Decterov, and A.D. Pelton: "Critical Thermodynamic Evaluation and Optimization of the CaO-MgO-SiO_2 System," *J. Eur. Ceram. Soc.,* 2003 (in press).
19. www.factsage.com, 2002.
20. I.-H. Jung, S.A. Decterov, and A.D. Pelton: "Thermodynamic Modeling of the CaO-MgO-Al_2O_3-SiO_2 System," in preparation.
21. G.A. Rankin and H.E. Merwin: "The Ternary System CaO-Al_2O_3-MgO," *J. Am. Chem. Soc.,* 1916, *38,* pp. 568-88.
22. A.M. Alper, R.N. McNally, P.H. Ribbe, and R.C. Doman: "The System MgO-$MgAl_2O_4$," *J. Am. Ceram. Soc.,* 1962, *45,* pp. 263-68.
23. D. Viechnicki, F. Schmid, and J.W. Mccauley: "Liquidus-Solidus Determinations in the System $MgAl_2O_4$-Al_2O_3," *J. Am. Ceram. Soc.,* 1974, *57,* pp. 47-48.
24. W.P. Whitney and V.S. Stubican: "Interdiffusion in the System MgO-$MgAl_2O_4$," *J. Am. Ceram. Soc.,* 1971, *54,* pp. 349-52.
25. V.S. Stubican and R. Roy: "Mechanism of the Precipitation of the Spinel from MgO-Al_2O_3 Solid Solutions," *J. Phys. Chem. Solids,* 1965, *26,* pp. 1293-97.
26. A.F. Henriksen and W.D. Kingery: "The Solid Solubility of Sc_2O_3, Al_2O_3, Cr_2O_3, SiO_2 and ZrO_2 in MgO," *Ceramurgia Int.,* 1979, *5,* pp. 11-17.
27. T. Mori: "Solubility of Aluminum Oxide in Magnesium Oxide," *Yogyo Kyokaishi,* 1982, *90,* pp. 551-52.
28. A.S. Frenkel, K.M. Shmukler, D.Ya. Sukharevskij, and N.V. Gul'ko: *Dokl. Akad. Nauk SSSR,* 1960, *130,* pp. 1095-98.
29. H.U.B. Viertel and F.K. Seifert: "Thermal Stability of Defect Spinels in the System $MgAl_2O_4$-Al_2O_3," *N. Jb. Miner. Abh.*, 1980, *140,* pp. 89-101.
30. A. Navrotsky, B. Wechsler, K. Geisinger, and F. Seifert: "Thermochemistry of $MgAl_2O_4$-$Al_{8/3}O_4$ Defect Spinels," *J. Am. Ceram. Soc.,* 1986, *69,* pp. 418-422.
31. A.M. Lejus: "Sur la Formation à Haute Température de Spinelles non Stoechiométriques et de Phases Dérivées," *Revue Int. Haut. Temp. Refract.,* 1964, *1,* pp. 53-95 (in French).
32. D.M. Roy, R. Roy, and E.F. Osborn: "The System MgO-Al_2O_3-H_2O and Influence of Carbonate and Nitrate Ions on the Phase Equilibria," *Am. J. Sci.,* 1953, *251,* pp. 337-61.
33. K. Shirasuka and G. Yamaguchi: "Precise Measurement of the Crystal Data and the Solid Solution Range of the Defective Spinel Magnesium Oxide.n (Aluminum Oxide)," *Yogyo Kyokaishi,* 1974, *82,* pp. 34-37.
34. H. Saalfeld and H. Jagodzinski: "Segregation of Mg-Al Spinels With an Excess of Al_2O_3," *Z. Krist.,* 1957, *109,* pp. 87-109.
35. A.M. Lejus and R. Collongues: "Sur la Formation à Haute Température de Phases Type Alumine δ dans Plusieurs Systemes à Base d'Alumine," *Acad. Sci.,* 1962, pp. 2780-2781 (in French).
36. Y. Chiang and W.D. Kingery: "Grain-Boundary Migration in

Nonstoichiometric Solid Solutions of Magnesium Aluminate Spinel: Grain Growth Studies," *J. Am. Ceram. Soc.,* 1989, *72,* pp. 271-77.
37. K. Fujii, T. Nagasaka, and M. Hino: *ISIJ Int.,* 2000, *40,* pp. 1059-66.
38. S.K. Roy and R.L. Coble: "Solubilities of Magnesia, Titania, and Magnesium Titanate in Aluminum Oxide," *J. Am. Ceram. Soc.,* 1968, *51,* pp. 1-6.
39. K. Ando and M. Momoda: "Solubility of Magnesium Oxide in Single-Crystal Aluminum Oxide," *J. Ceram. Soc. Jpn. Int. Ed.,* 1987, *95,* pp. 343-47.
40. E.G. King: "Heat Capacities at Low Temperatures and Entropies at 298.16 K of Crystalline Calcium and Magnesium Aluminates," *J. Phys. Chem.,* 1955, *59,* pp. 218-19.
41. K.R. Bonnickson: "High Temperature Heat Contents of Aluminates of Calcium and Magnesium," *J. Phys. Chem.,* 1955, *59,* pp. 220-21.
42. Ya.A. Landa and I.A. Naumova: "Determining the Enthalpy and Specific Heat of Magnesia Spinels in the Range 1400-2200 K," *Ogneupory,* 1979, pp. 9-12.
43. P. Richet and G. Fiquet: "High-Temperature Heat Capacity and Premelting of Minerals in the System MgO-CaO-Al_2O_3-SiO_2," *J. Geophys. Res.,* 1991, *96,* pp. 445-56.
44. T.V. Charlu, R.C. Newton, and O.J. Kleppa: "Enthalpies of Formation of 970 K of Compounds in the System Magnesia-Alumina Silica from High Temperature Solution Calorimetry," *Geochim. Cosmochim. Acta,* 1975, *39,* pp. 1487-97.
45. J.A. Shearer and O.J. Kleppa: "Enthalpies of Formation of Spinel ($MgAl_2O_4$), Pyroxene ($MgSiO_3$), Olivine (Mg_2SiO_4), Kyanite (Al_2SiO_5), and Sillimanite (Al_2SiO_5) by Oxide Melt Solution Calorimetry," *J. Inorg. Nucl. Chem.,* 1973, *35*, pp. 1073-78.
46. A. Navrotsky and O.J. Kleppa: "Thermodynamics of Formation of Simple Spinels," *J. Inorg. Nucl. Chem.,* 1968, *30,* pp. 479-98.
47. K.T. Jacob and K.P.W.Y. Jayadevan: "Electrochemical Determination of the Gibbs Energy of Formation of $MgAl_2O_4$," *J. Am. Ceram. Soc.,* 1998, *81,* pp. 209-12.
48. L. Chamberlin, J.R. Beckett, and E. Stolper: "Palladium Oxide Equilibration and the Thermodynamic Properties of $MgAl_2O_4$ Spinel," *Am. Mineral.,* 1995, *80,* pp. 285-96.
49. R.W. Taylor and H. Schmalzried: "The Free Energy of Formation of Some Titanates, Silicates, and Magnesium Aluminate From Measurements Made With Galvanic Cells Involving Solid Electrolytes," *J. Phys. Chem.,* 1964, *68,* pp. 2444-49.
50. E. Rosen and A. Muan: "Stability of $MgAl_2O_4$ at 1400°C as Derived from Equilibrium Measurements in $CoAl_2O_4$-$MgAl_2O_4$ Solid Solutions," *J. Am. Ceram. Soc.,* 1966, *49,* pp. 107-08.
51. K. Grjøtheim, O. Herstad, and J.M. Toguri: *Can. J. Chem.* 1961, *39,* pp. 443-50.
52. R.L. Altman: "Vaporization of Magnesium Oxide and its Reaction with Alumina," *J. Phys. Chem.,* 1963, *67,* pp. 366-69.
53. T. Sasamoto, H. Hara, and T. Sata: "Mass-Spectrometric Study of the Vaporization of Magnesium Oxide from Magnesium Aluminate Spinel," *Bull. Chem. Soc. Jpn.,* 1981, *54,* pp. 3327-33.
54. J.M. McHale, A. Auroux, A.J. Perrotta, and A. Navrotsky: "Surface Energies and Thermodynamic Phase Stability in Nanocrystalline Aluminas," *Science (Washington, DC),* 1997, *277,* pp. 788-91.
55. T. Yamanaka and Y. Takeuchi: "Order-Disorder Transition in $MgAl_2O_4$ Spinel at High Temperatures up to 1700 °C," *Z. Kristallogr.,* 1983, *165,* pp. 65-78.
56. R.C. Peterson, G.A. Lager, and R.L. Hitterman: "A Time-of-Flight Neutron Powder Diffraction Study of $MgAl_2O_4$ at Temperature up to 1273 K," *Am. Mineral.,* 1991, *76,* pp. 1455-58.
57. S.A.T. Redfern, R. Harrison, H.St.C. O'Neill, and D.R.R. Wood: "Thermodynamics and Kinetics of Cation Ordering in $MgAl_2O_4$ Spinel up to 1600 °C from in Situ Neutron Diffraction," *Am. Mineral.,* 1999, *84,* pp. 299-310.
58. H. Maekawa, S. Kato, K. Kawamura, and T. Yokokawa: "Cation Mixing in Natural $MgAl_2O_4$ Spinel: A High-Temperature 27Al NMR Study," *Am. Mineral.,* 1997, *82,* pp. 1125-32.
59. B.J. Wood, R.J. Kirkpatrick, and B. Montez: "Order-Disorder Phenomena in $MgAl_2O_4$ Spinel," *Am. Mineral.,* 1986, *71,* pp. 999-1006.
60. R.L. Millard, R. Peterson, and B.K. Hunter: "Temperature Dependence of Cation Disorder in $MgAl_2O_4$ Spinel Using 27Al and 17O Magic-Angle Spinning NMR," *Am. Mineral.,* 1992, *77,* pp. 44-52.
61. G.B. Andreozzi, F. Princivalle, H. Skogby, and A.D. Giusta: "Cation Ordering and Structural Variations With Temperature in $MgAl_2O_4$ Spinel: An X-ray Single-Crystal Study," *Am. Mineral.,* 2000, *85,* pp. 1164-71.
62. A. Navrotsky: "Cation Distribution Energies and Heats of Mixing in $MgFe_2O_4$-$MgAl_2O_4$-$ZnFe_2O_3$-$ZnAl_2O_4$, and $NiAl_2O_4$-$ZnAl_2O_4$ Spinels: Study by High-Temperature Calorimetry," *Am. Mineral.,* 1986, *71,* pp. 1160-69.
63. K. Grjotheim, O. Herstad, and J.M. Toguri: "The Aluminum Reduction of Magnesium Compounds," *Can. Min. Metall.,* 1962, pp. 396-99.
64. J.H. Welch: "Ternary Compound Formation in the System CaO-Al_2O_3-MgO," *Nature,* 1961, *4788,* pp. 559-60.
65. A.J. Majumdar: "The Quaternary Phase in High-Alumina Cement," *Trans. J Br. Ceram. Soc.,* 1964, *63,* pp. 347-64.
66. M.R. Rao: "Liquidus Relations in the Quaternary Subsystem $CaAl_2O_4$-$CaAl_4O_7$-$Ca_2Al_2SiO_7$-$MgAl_2O_4$," *J. Am. Ceram. Soc.,* 1968, *51,* pp. 50-54.
67. M.T. Melnik, A.A. Kachura, and N.V. Mokritskaya: "Phase Diagram of the Calcium Aluminate-Magnesium Aluminate-Magnesia (CaO-Al_2O_3-MgO-Al_2O_3-MgO," *Ogneupory,* 1989, *4,* pp. 27-28.
68. A.H. De Aza, P. Pena, and S. De Aza: "Ternary System Al_2O_3-MgO-CaO: I: Primary Phase Field of Crystallization of Spinel in the Subsystem $MgAl_2O_4$-$CaAl_4O_7$-CaO-MgO," *J. Am. Ceram. Soc.,* 1999, *82,* pp. 2193-203.
69. A.H. De Aza, J.E. Iglesias, P. Pena, and S. De Aza: "Ternary System Al_2O_3-MgO-CaO: Part II, Phase Relationships in the Subsystem Al_2O_3-$MgAl_2O_4$-$CaAl_4O_7$," *J. Am. Ceram. Soc.,* 2000, *83,* pp. 919-27.
70. M. Göbbels, E. Woermann, and J. Jung: "The Al-Rich Part of the System CaO-Al_2O_3-MgO. Part I. Phase Relationships," *J. Solid State Chem.,* 1995, *120,* pp. 358-63.
71. N. Iyi, M. Göbbels, and Y. Matsui: "The Al-Rich Part of the System CaO-Al_2O_3-MgO. Part II. Structure Refinement of Two New Magnetoplumbite-Related Phases," *J. Solid State Chem.,* 1995, *120,* pp. 364-71.
72. H. Ohta and H. Suito: "Activities in CaO-MgO-Al_2O_3 Slags and Deoxidation Equilibria of Al, Mg, and Ca," *ISIJ,* 1996, *36,* pp. 983-90.
73. M. Hino, S. Kinoshita, Y. Ehara, H. Itoh, and S. Ban-Ya: "Activity Measurement of the Constituents in Secondary Steelmaking Slag" in *Proc. 5th Int. Sympos. Metall. Slags and Fluxes*, 1997, pp. 53-57.
74. M. Allibert, C. Chatillon, and R. Lourtau: *Rev Int. Hautes Temp. Refract.,* 1979, *16*, pp. 33-37.
75. R.W. Nurse, J.H. Welch, and A.J. Majumdar: "The CaO-Al_2O_3 System in a Moisture-Free Atmosphere," *Trans. Brit. Ceram. Soc.,* 1965, *64,* pp. 409-18.

76. J.W. Greig: "Immiscibility in Silicate Melts. Part I," *Am. J. Sci., 5th Ser.,* 1927, *13,* pp. 1-44.
77. G.A. Rankin and H.E. Merwin: "The Ternary System MgO-Al_2O_3-SiO_2," *Am. J. Sci.,* 1918, *45,* pp. 301-25.
78. W. Schreyer and J.F. Schairer: "Stable and Metastable Phase Relations in the System MgO-Al_2O_3-SiO_2," *Carnegie Inst. of Washington,* 1961, *Yb. 60,* pp. 144-47.
79. W.J. Schreyer and J.F. Schairer: "Compositions and Structural States of Anhydrous Mg-Cordierites: A Re-investigation of the Central Part of the System MgO-Al_2O_3-SiO_2," *J. Petrol.,* 1961, *2,* pp. 324-406.
80. M.L. Keith and J.F. Schairer: "The Stability Field of Sapphirine in the System MgO-Al_2O_3-SiO_2," *J. Geol.,* 1952, *60,* pp. 181-86.
81. S. Aramaki and R. Roy: "The Mullite-Corundum Boundary in the Systems MgO-Al_2O_3-SiO_2 and CaO-Al_2O_3-SiO_2," *J. Am. Ceram. Soc.,* 1961, *42,* pp. 644-45.
82. C.M. Schlaudt and D.M. Roy: "Crystalline Solution in the System MgO-Mg_2SiO_4-$MgAl_2O_4$," *J. Am. Ceram. Soc.,* 1965, *48,* pp. 248-51.
83. K. Onuma and M. Arita: "Magnesium Silicate-Magnesium Aluminum Silicate ($MgSiO_3$-$MgAl_2SiO_6$) Join and the Solubility of Aluminum Oxide in Enstatite at Atmospheric Pressure," *Ganseki Kobutsu Kosho Gakkaishi,* 1975, *70,* pp. 53-60.
84. P. Anastasiou and F. Seifert: "Solid Solubility of Aluminum Oxide in Enstatite at High Temperatures and 1-5 kbars Water Pressure," *Contrib. Mineral. Petrol.,* 1972, *34,* pp. 272-87.
85. R.M. Smart and F.P. Glasser: "The Subsolidus Phase Equilibria and Melting Temperatures of MgO-Al_2O_3-SiO_2 Compositions," *Ceram. Int.,* 1981, *7,* pp. 90-97.
86. E.F. Osborn and A. Muan: *Phase Equilibrium Diagrams of Oxide Systems,* The American Ceramic Society and the Edward Orton Jr. Ceramic Foundation, Columbus, OH, 1960.
87. W.R. Foster: "Synthetic Sapphirine and Its Stability Relations in the System MgO-Al_2O_3-SiO_2," *J. Am. Ceram. Soc.,* 1950, *33,* pp. 73-84.
88. S. Sakai and T. Kawasaki: "Phase Relations for $Mg_3Al_2Si_3O_{12}$ (Pyrope Composition) in the System MgO-Al_2O_3-SiO_2 at Atmospheric Pressure," *Ganko,* 1998, *93*, pp. 18-26.
89. R.M. Smart and F.P. Glasser: "Phase Relations of Cordierite and Sapphirine in the System MgO-Al_2O_3-SiO_2," *J. Mater. Sci.,* 1976, *11,* pp. 1459-64.
90. W.W. Weller and K.K. Kelley: "Low-Temperature Heat Capacities and Entropies at 298.15 K of Akermanite, Cordierite, Gehlenite, and Merwinite," U.S. Bureau of Mines, Report of Investigation, 1963.
91. C.A. Geiger and H. Voigtlander: "The Heat Capacity of Synthetic Anhydrous Mg and Fe Cordierite," *Contrib. Mineral. Petrol.,* 2000, *138,* pp. 46-50.
92. R. Mueller, R. Naumann, and S. Reinsch: "Surface Nucleation of μ.-Cordierite in Cordierite Glass: Thermodynamic Aspects," *Thermochim. Acta,* 1996, *280/281(Vitrification, Transformation and Crystallization of Glasses),* pp. 191-204.
93. B.N. Roy and A. Navrotsky: "Thermochemistry of Charge-Coupled Substitutions in Silicate Glasses: The Systems $MAlO_2$-SiO_2 (M = Li,Na,K,Rb,Cs,Mg,Ca,Sr,Ba,Pb)," *J. Am. Ceram. Soc.,* 1984, *67,* pp. 606-10.
94. P. Courtial and P. Richet: "Heat Capacity of Magnesium Aluminosilicate Melts," *Geochim. Cosmochim. Acta,* 1993, *57,* pp. 1267-75.
95. R.H. Rein and J. Chipman: "Activities in the Liquide Solution SiO_2-CaO-MgO-Al_2O_3 at 1600 °C," *TMS-AIME,* 1965, *233,* pp. 415-25.
96. D. Henderson and J. Taylor: "Thermodynamic Properties in the CaO-MgO-SiO_2 and MgO-Al_2O_3-SiO_2 Systems," *J. Iron Steel Inst., 204,* 1966, pp. 41-45.
97. R.G. Berman: "Internally-Consistent Thermodynamic Data for Minerals in the System Sodium Oxide-Potassium Oxide-Calcium Oxide-Magnesium Oxide-Iron Oxide(FeO)-Iron Oxide(Fe_2O_3)-Alumina-Silica-Titania-Water-Carbon Dioxide," *J. Petrol.,* 1988, *29,* pp. 445-522.
98. S. Aramaki and R. Roy: *J. Am. Ceram. Soc.,* 1959, *42,* pp. 644-45.
99. A.T. Prince: "Liquidus Relations on 10% MgO Plane of the System Lime-Magnesia-Alumina-Silica," *J. Am. Ceram. Soc.,* 1954, *37,* pp. 402-08.